

Bayesian group latent factor analysis with structured sparse priors

Shiwen Zhao

*Computational Biology and Bioinformatics
Duke University
Durham, NC 27705, USA*

SHIWEN.ZHAO@DUKE.EDU

Chuan Gao

*Department of Statistical Science
Duke University
Durham, NC 27705, USA*

CHUAN.GAO@DUKE.EDU

Sayan Mukherjee

*Department of Statistical Science
Duke University
Durham, NC 27705, USA*

SAYAN@STAT.DUKE.EDU

Barbara E Engelhardt

*Department of Computer Science
Princeton University
Princeton, NJ 08540, USA*

BEE@PRINCETON.EDU

Abstract

Latent factor models are the canonical statistical tool for exploratory analyses of low-dimensional linear structure for an observation matrix with p features across n samples. We develop a Bayesian group factor analysis (BGFA) model that extends the factor model to multiple coupled observation matrices. Our model puts a structured Bayesian hierarchical prior on the joint factor loading matrix, which achieves shrinkage effect at both a local level (element-wise shrinkage) and a factor level (column-wise shrinkage) with non-parametric behavior that removes unnecessary factors. With two observations, our model reduces to Bayesian canonical correlation analysis (BCCA). We exploit the shrinkage behavior in the BGFA model to recover covariance structure across all subsets of the observation matrices where this signal exists. We validate our model on simulated data with substantial structure and compare recovered factor loadings against results from related methods. We then show the results of applying BGFA to two genomics studies for different analytic aims: identifying gene co-expression networks specific to one of two conditions, and recovering sets of genetic variants that jointly regulate transcription of a collection of genes. We illustrate the unique ability of BGFA to use multiple observations of the same samples to guide linear projection of the data onto a latent space, producing meaningful and robust low-dimensional representations, as compared with ‘unsupervised’ projections from traditional factor analysis or principal components analysis.

Keywords: Bayesian Structured Sparsity, Canonical Correlation Analysis, Sparse Priors, Mixture Models, Statistical Association

1. Introduction

Factor analysis models have attracted attention recently due to their ability to perform interpretable exploratory analyses of high dimensional data rapidly (West, 2003; Carvalho et al., 2008; Engelhardt and Stephens, 2010). A latent factor model finds a low dimensional representation $\mathbf{x}_i \in \mathbb{R}^{k \times 1}$ of a high dimensional observation of p features, $\mathbf{y}_i \in \mathbb{R}^{p \times 1}$ for n samples. A observation in the low dimensional space is linearly projected to the original high dimensional space through a *loadings matrix* $\mathbf{\Lambda} \in \mathbb{R}^{p \times k}$ with Gaussian noise $\boldsymbol{\epsilon}_i \in \mathbb{R}^{p \times 1}$:

$$\mathbf{y}_i = \mathbf{\Lambda} \mathbf{x}_i + \boldsymbol{\epsilon}_i, \tag{1}$$

for $i = 1, \dots, n$. It is often assumed, as we do here, that \mathbf{x}_i follows a $\mathcal{N}_k(\mathbf{0}, \mathbf{I}_k)$ distribution, where \mathbf{I}_k is the identity matrix of dimension k , and $\boldsymbol{\epsilon}_i \sim \mathcal{N}_p(\mathbf{0}, \boldsymbol{\Sigma})$, where $\boldsymbol{\Sigma}$ is a $p \times p$ diagonal covariance matrix with σ_j^2 for $j = 1, \dots, p$ on the diagonal. In many applications of factor analysis, the number of latent factors k is much smaller than the number of features p and the number of samples n . By integrating over the factor \mathbf{x}_i , the factor analysis model produces a low-rank estimation of the covariance matrix associated with the features. In particular, the covariance of \mathbf{y}_i , $\boldsymbol{\Omega} \in \mathbb{R}^{p \times p}$, is written as

$$\boldsymbol{\Omega} = \mathbf{\Lambda} \mathbf{\Lambda}^T + \boldsymbol{\Sigma} = \sum_{h=1}^k \boldsymbol{\lambda}_h \boldsymbol{\lambda}_h^T + \boldsymbol{\Sigma}, \tag{2}$$

where $\boldsymbol{\lambda}_h$ is the h^{th} column of $\mathbf{\Lambda}$. This factorization suggests that each factor separately contributes to the covariance of the observation through its corresponding loading. Traditional exploratory data analysis methods such as principle component analysis (PPCA) (Hotelling, 1933), independent component analysis (ICA) (Comon, 1994), and canonical correlation analysis (CCA) (Hotelling, 1936) all have interpretations as latent factor models. Indeed, the field of latent linear models is extremely broad, and robust unifying frameworks are desirable (Cunningham and Ghahramani, 2014).

The loading matrix $\mathbf{\Lambda}$ plays an important role in the subspace mapping. In applications where there are fewer samples than features in the observed data, the $n < p$ scenario, it is essential to include strong regularization on the loading matrix due to the fact that this optimization problem is under-constrained and has many equivalent solutions that optimize the likelihood function. In the machine learning and statistics literature, priors or penalties are used to regularize the elements of the loading matrix, occasionally by inducing sparsity. Element-wise sparsity corresponds to *feature selection*. Sparsity eliminates the contribution of some features to a factor, with the effect that a latent factor contributes to variation in only a subset of the observed features (West, 2003; Carvalho et al., 2008; Knowles and Ghahramani, 2011). In gene expression data, sparse factor loadings are interpreted as clusters of genes and used to identify sets of co-regulated genes (Pournara and Wernisch, 2007; Lucas et al., 2010; Gao et al., 2013).

Imposing element-wise sparsity in factor models has been studied through regularization via L_1 type penalties in classical statistics (Zou et al., 2006; Witten et al., 2009; Salzman et al., 2010). More recently, Bayesian shrinkage methods using sparsity-inducing priors have been introduced for latent factor models (Archanbeau and Bach, 2008; Carvalho et al., 2008; Virtanen et al., 2011; Bhattacharya and Dunson, 2011; Klami et al., 2013). In contrast to

regularization methods from classical statistics, Bayesian shrinkage has the advantage of being adaptive to data and borrowing information across groups using hierarchical parameterizations. To achieve shrinkage effects, a prior distribution should have substantial probability mass around zero; at the same time it should have heavy tails to allow signals to escape from shrinkage (O’Hagan, 1979; Polson and Scott, 2010; Carvalho et al., 2010). The spike-and-slab prior (Mitchell and Beauchamp, 1988), the classic two-group Bayesian sparsity-inducing prior, has been used for sparse Bayesian latent factor models (Carvalho et al., 2008). A more computationally tractable one-group prior, the automatic relevance determination (ARD) prior (Neal, 1995; Tipping, 2001), has also been used to induce sparsity in latent factor models (Engelhardt and Stephens, 2010; Pruteanu-Malinici et al., 2011).

Another active area of research in latent factor models focuses on incorporating structure in the loading matrix. Built on canonical correlation analysis (CCA), which takes paired feature vectors $\mathbf{y}_i^{(1)} \in \mathbb{R}^{p_1 \times 1}$ and $\mathbf{y}_i^{(2)} \in \mathbb{R}^{p_2 \times 1}$ for the same n samples and identifies a linear latent space for which the correlations between the two observations are maximized, the Bayesian CCA (BCCA) model (Klami et al., 2013) assumes a latent factor model for each observation through a shared latent vector $\mathbf{x}_i \in \mathbb{R}^{k \times 1}$. This Bayesian CCA model may be written as a latent factor model by vertical concatenation of observations, loading matrices, and Gaussian residual errors. By inducing group-wise sparsity—explicit blocks of zeros—in the combined loading matrix, the covariance across two observations and covariance local to each observation may be estimated (Klami and Kaski, 2008; Klami et al., 2013). Extensions of this approach to multiple coupled observations $\mathbf{y}_i^{(1)} \in \mathbb{R}^{p_1 \times 1}, \dots, \mathbf{y}_i^{(m)} \in \mathbb{R}^{p_m \times 1}$ have resulted in group factor analysis models (GFA) (Archambeau and Bach, 2008; Salzmann et al., 2010; Jia et al., 2010; Virtanen et al., 2011). Beyond group-wise sparsity, more sophisticated structured regularizations have been studied in classical statistics (Zou and Hastie, 2005; Kowalski and Torrsani, 2009; Jenatton et al., 2011; Huang et al., 2011).

Latent factor models (Equation (1)) may be interpreted as capturing a low-rank estimate of the feature covariance matrix. BCCA extends this covariance representation to two observations. Group-wise sparsity in the combined loading matrix jointly models covariance structure shared across both observations and covariance local to each observation. GFA further extends this representation to m observations for the same samples, modeling, in its fullest generality, the covariance associated with every subset of observations. Thus, GFA becomes intractable when m is large: the number of covariance matrices for all subsets of the m observations increases exponentially in m .

In this study, we incorporate Bayesian shrinkage with hierarchical structure to develop a flexible Bayesian GFA (BGFA) model with non-parametric behavior that enables us to avoid this curse of dimensionality. We leveraged a recently developed hierarchical sparsity-inducing prior that has a computationally tractable representation as a scale mixture of normals, the three parameter Beta prior (\mathcal{TPB}) (Armagan et al., 2011b; Gao et al., 2013). We developed a structured hierarchical shrinkage prior to enable the application of BGFA to multiple high dimensional observation matrices. Our BGFA model has many desirable properties: i) it shrinks the loading matrix globally, removing unnecessary factors and inducing non-parametric behavior where the number of factors is driven by the data; ii) it allows factor loadings to have either a sparsity-inducing or a dense regularization prior, enabling a factor to correspond either to a subset of features or to all features; iii) it only

estimates covariance matrices for which there is sufficient signal, exploiting non-parametric behavior to skirt the curse of dimensionality in GFA models.

In this paper, we discuss current work in sparse latent factor models and describe our BGFA model in Section (2). Then we briefly review Bayesian shrinkage priors and introduce the structured hierarchical prior in our BGFA model in Sections (3) and (4). In Section (5), we describe how we perform parameter estimation. In Section (6) we illustrate the performance of our model on the task of recovering simulated sparse signals among m observation matrices with substantial structures. We then present results that illustrate the performance of our model on real world data in Section (7). In particular, we show that our model recovers condition-specific co-regulated gene networks in two gene expression level observations from cells that had been exposed to a drug versus saline solution. Then we illustrate how our model may be applied to the problem of identifying groups of genes that are regulated by genetic variants in a large, publicly available genomic data set. We conclude by considering possible extensions to this model in Section (8).

2. Bayesian Group Factor Model

2.1 Latent Factor Models

Factor analysis has been extensively used in dimension reduction and low dimensional covariance matrix estimation. For concreteness, we write the basic factor analysis model as

$$\mathbf{y}_i = \mathbf{\Lambda}\mathbf{x}_i + \boldsymbol{\epsilon}_i,$$

where $\mathbf{y}_i \in \mathbb{R}^{p \times 1}$ is modeled as a linear transformation of a latent vector $\mathbf{x}_i \in \mathbb{R}^{k \times 1}$ through loading matrix $\mathbf{\Lambda} \in \mathbb{R}^{p \times k}$ (Figure 1A). Here, \mathbf{x}_i is assumed to follow a $\mathcal{N}_k(\mathbf{0}, \mathbf{I}_k)$ distribution, where \mathbf{I}_k is the k -dimensional identity matrix, and $\boldsymbol{\epsilon}_i \sim \mathcal{N}_p(\mathbf{0}, \boldsymbol{\Sigma})$, where $\boldsymbol{\Sigma}$ is a $p \times p$ diagonal matrix. With an isotropic noise assumption, $\boldsymbol{\Sigma} = \mathbf{I}\sigma^2$; this model has a probabilistic principal components analysis interpretation (Roweis, 1998; Tipping and Bishop, 1999b). For factor analysis, and in this work, it is assumed that $\boldsymbol{\Sigma} = \text{diag}(\sigma_1^2, \dots, \sigma_p^2)$ representing independent idiosyncratic noise (Tipping and Bishop, 1999a).

Integrating over the factors \mathbf{x}_i , we see that the covariance of \mathbf{y}_i is estimated with a low rank matrix factorization: $\mathbf{\Lambda}\mathbf{\Lambda}^T + \boldsymbol{\Sigma}$. We further let $\mathbf{Y} = [\mathbf{y}_1, \dots, \mathbf{y}_n]$ be the collection of n samples of \mathbf{y}_i , and similarly let $\mathbf{X} = [\mathbf{x}_1, \dots, \mathbf{x}_n]$ and $\mathbf{E} = [\boldsymbol{\epsilon}_1, \dots, \boldsymbol{\epsilon}_n]$. Then the factor analysis model for the observation \mathbf{Y} is

$$\mathbf{Y} = \mathbf{\Lambda}\mathbf{X} + \mathbf{E}.$$

2.2 Probabilistic Canonical Correlation Analysis

In the context of two paired observations $\mathbf{y}_i^{(1)} \in \mathbb{R}^{p_1 \times 1}$ and $\mathbf{y}_i^{(2)} \in \mathbb{R}^{p_2 \times 1}$ on the same n samples, canonical correlation analysis (CCA) seeks to find linear projections (canonical directions) such that the sample correlations in the projected space are mutually maximized (Hotelling, 1936). The work of interpreting CCA as a probabilistic model can be traced back to classical descriptions by Bach and Jordan (2005). With a common latent

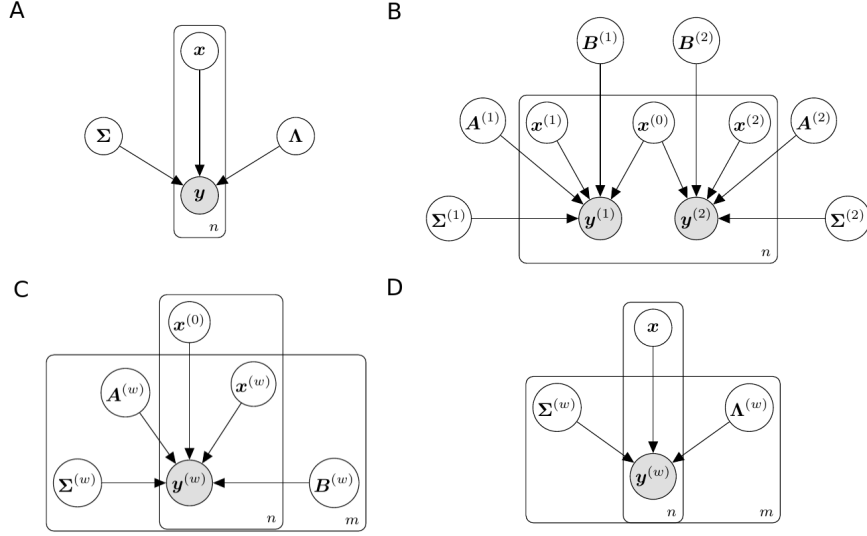


Figure 1: **Graphical representations of different latent factor models.** Panel A: Factor analysis model. Panel B: Bayesian canonical correlation analysis model (BCCA). Panel C: Group factor analysis (GFA) model with block diagonal structure. Panel D: Bayesian group factor analysis (BGFA) model proposed in this study.

factor, $\mathbf{x}_i \in \mathbb{R}^{k \times 1}$, $\mathbf{y}_i^{(1)}$ and $\mathbf{y}_i^{(2)}$ are modelled as

$$\begin{aligned} \mathbf{y}_i^{(1)} &= \mathbf{\Lambda}^{(1)} \mathbf{x}_i + \mathbf{e}_i^{(1)}, \\ \mathbf{y}_i^{(2)} &= \mathbf{\Lambda}^{(2)} \mathbf{x}_i + \mathbf{e}_i^{(2)}. \end{aligned} \quad (3)$$

The errors are distributed as $\mathbf{e}_i^{(1)} \sim \mathcal{N}_{p_1}(\mathbf{0}, \mathbf{\Psi}^{(1)})$ and $\mathbf{e}_i^{(2)} \sim \mathcal{N}_{p_2}(\mathbf{0}, \mathbf{\Psi}^{(2)})$, where $\mathbf{\Psi}^{(1)}$ and $\mathbf{\Psi}^{(2)}$ are positive semi-definite matrices, which are not necessarily diagonal, allowing dependencies among residual errors within an observation. The maximum likelihood estimates of the loading matrices, $\mathbf{\Lambda}^{(1)}$ and $\mathbf{\Lambda}^{(2)}$, are the first k canonical directions up to orthogonal transformation (Bach and Jordan, 2005).

2.3 Bayesian CCA with Group-wise Sparsity

Building on the probabilistic CCA model, a Bayesian CCA (BCCA) model proposed by Klami et al. (2013) has the following form

$$\begin{aligned} \mathbf{y}_i^{(1)} &= \mathbf{A}^{(1)} \mathbf{x}_i^{(0)} + \mathbf{B}^{(1)} \mathbf{x}_i^{(1)} + \boldsymbol{\epsilon}_i^{(1)}, \\ \mathbf{y}_i^{(2)} &= \mathbf{A}^{(2)} \mathbf{x}_i^{(0)} + \mathbf{B}^{(2)} \mathbf{x}_i^{(2)} + \boldsymbol{\epsilon}_i^{(2)}, \end{aligned} \quad (4)$$

with $\mathbf{x}_i^{(0)} \in \mathbb{R}^{k_0 \times 1}$, $\mathbf{x}_i^{(1)} \in \mathbb{R}^{k_1 \times 1}$ and $\mathbf{x}_i^{(2)} \in \mathbb{R}^{k_2 \times 1}$ (Figure 1B). The latent vector $\mathbf{x}_i^{(0)}$ is shared by both $\mathbf{y}_i^{(1)}$ and $\mathbf{y}_i^{(2)}$, and captures their common variation through loading matrices $\mathbf{A}^{(1)}$ and $\mathbf{A}^{(2)}$. Two additional latent vectors, $\mathbf{x}_i^{(1)}$ and $\mathbf{x}_i^{(2)}$, are specific to each observation; they are multiplied by observation-specific loading matrices $\mathbf{B}^{(1)}$ and $\mathbf{B}^{(2)}$. The two residual

error terms are $\epsilon_i^{(1)} \sim \mathcal{N}_{p_1}(\mathbf{0}, \Sigma^{(1)})$ and $\epsilon_i^{(2)} \sim \mathcal{N}_{p_2}(\mathbf{0}, \Sigma^{(2)})$, where $\Sigma^{(1)}$ and $\Sigma^{(2)}$ are two diagonal matrices. This model was originally called Inter-Battery Factor Analysis (IBFA) (Browne, 1979) and recently has been studied under a full Bayesian inference framework (Klami et al., 2013). This model can be viewed as a probabilistic CCA model (Equation (3)) with an additional low rank factorization of the error covariance matrices. In particular, we re-write the residual error term specific to observation w ($w = 1, 2$) from the probabilistic CCA model (Equation (3)) as $e_i^{(w)} = \mathbf{B}^{(w)}\mathbf{x}_i^{(w)} + \epsilon_i^{(w)}$; then marginally $e_i^{(w)} \sim \mathcal{N}_{p_w}(\mathbf{0}, \Psi^{(w)})$ where $\Psi^{(w)} = \mathbf{B}^{(w)}(\mathbf{B}^{(w)})^T + \Sigma^{(w)}$.

Klami et al. (2013) re-wrote model (4) as a factor analysis model with group-wise sparsity in the loading matrix. Let $\mathbf{y}_i \in \mathbb{R}^{p \times 1}$ with $p = p_1 + p_2$ be the vertical concatenation of $\mathbf{y}_i^{(1)}$ and $\mathbf{y}_i^{(2)}$; let $\mathbf{x}_i \in \mathbb{R}^{k \times 1}$ with $k = k_0 + k_1 + k_2$ be vertical concatenation of $\mathbf{x}_i^{(0)}$, $\mathbf{x}_i^{(1)}$ and $\mathbf{x}_i^{(2)}$; and let $\epsilon_i \in \mathbb{R}^{p \times 1}$ be vertical concatenation of the two residual errors. Then, the BCCA model in Equation (4) can be written as a factor analysis model

$$\mathbf{y}_i = \mathbf{\Lambda}\mathbf{x}_i + \epsilon_i,$$

with $\epsilon_i \sim N_p(\mathbf{0}, \Sigma)$, where

$$\mathbf{\Lambda} = \begin{bmatrix} \mathbf{A}^{(1)} & \mathbf{B}^{(1)} & \mathbf{0} \\ \mathbf{A}^{(2)} & \mathbf{0} & \mathbf{B}^{(2)} \end{bmatrix}, \Sigma = \begin{bmatrix} \Sigma^{(1)} & \mathbf{0} \\ \mathbf{0} & \Sigma^{(2)} \end{bmatrix}. \quad (5)$$

The structure in the loading matrix $\mathbf{\Lambda}$ has a specific meaning: the non-zero columns (those in $\mathbf{A}^{(1)}$ and $\mathbf{A}^{(2)}$) project the shared latent factors (i.e., the first k_0 in \mathbf{x}_i) to $\mathbf{y}_i^{(1)}$ and $\mathbf{y}_i^{(2)}$, respectively; these latent factors represent the covariance across the observations. The columns with zero blocks (those in $[\mathbf{B}^{(1)}; \mathbf{0}]$ or $[\mathbf{0}; \mathbf{B}^{(2)}]$) relate specific factors to only one of the two observations; they model covariance specific to that observation. Under this BCCA model, the structure of $\mathbf{\Lambda}$ is fixed *a priori*, and the inference problem is to estimate the values of the non-zero blocks of $\mathbf{\Lambda}$.

2.4 Group Factor Analysis Models

Group factor analysis (GFA) models have been proposed recently for the joint analysis of multiple ($m > 2$) coupled observations, $\mathbf{y}_i^{(1)} \in \mathbb{R}^{p_1 \times 1}, \dots, \mathbf{y}_i^{(m)} \in \mathbb{R}^{p_m \times 1}$ (Salomatin et al., 2009; Jia et al., 2010; Virtanen et al., 2011; Archambeau and Bach, 2008). GFA models are motivated by multi-view learning: these models partition the latent space into factors shared across all observations and factors private to each of the observations (Archambeau and Bach, 2008; Salzmann et al., 2010) (Figure 1C):

$$\mathbf{y}_i^{(w)} = \mathbf{A}^{(w)}\mathbf{x}_i^{(0)} + \mathbf{B}^{(w)}\mathbf{x}_i^{(w)} + \epsilon_i^{(w)} \quad \text{for } w = 1, \dots, m. \quad (6)$$

By vertical concatenation of $\mathbf{y}_i^{(w)}$, $\mathbf{x}_i^{(w)}$ and $\epsilon_i^{(w)}$, this model can be viewed as a latent factor model with loading matrix $\mathbf{\Lambda}$ having a similar group-wise sparsity pattern as in the BCCA model

$$\mathbf{\Lambda} = \begin{bmatrix} \mathbf{A}^{(1)} & \mathbf{B}^{(1)} & \dots & \mathbf{0} \\ \mathbf{A}^{(2)} & \mathbf{0} & \dots & \mathbf{0} \\ \vdots & \vdots & \ddots & \vdots \\ \mathbf{A}^{(m)} & \mathbf{0} & \dots & \mathbf{B}^{(m)} \end{bmatrix}. \quad (7)$$

Here, the first block column ($\mathbf{A}^{(w)}$) is a non-zero loading matrix across the features of all observations, and the remaining columns have a block diagonal structure with observation-specific loading matrices ($\mathbf{B}^{(w)}$) on the diagonal.

This GFA model is limited by the strict diagonal structure of the loading matrix. Structuring the loading matrix in this way prevents this model from capturing covariance structure among arbitrary subsets of observations. But, modeling covariance structure among all possible subsets of observations is non-trivial for large m because there are $2^m - 1$ possible subsets.

The GFA structure on $\mathbf{\Lambda}$ in Equation (7) has been relaxed to model covariance among subsets of the observations (Jia et al., 2010; Virtanen et al., 2011). In this formulation, each observation $\mathbf{y}_i^{(w)}$ is modeled by its own loading matrix $\mathbf{\Lambda}^{(w)}$ and a shared latent vector \mathbf{x}_i (Figure 1D):

$$\mathbf{y}_i^{(w)} = \mathbf{\Lambda}^{(w)} \mathbf{x}_i + \boldsymbol{\epsilon}_i^{(w)} \quad \text{for } w = 1, \dots, m. \quad (8)$$

By allowing columns in $\mathbf{\Lambda}^{(w)}$ to be zero, the model decouples certain latent factors from a subset of observations. The covariance structure of an arbitrary subset of observations is modeled by factors with non-zero loading columns corresponding to the observations in that subset. Factors that correspond to non-zero entries for only one observation capture covariance specific to that observation.

Two different approaches have been proposed to achieve this column-wise shrinkage effect: Bayesian shrinkage (Virtanen et al., 2011; Klami et al., 2013) and explicit penalties (Jia et al., 2010). The Bayesian shrinkage method puts a normal-inverse gamma prior, known as the automatic relevance determination (ARD) prior (Tipping, 2001), on each column of the m loading matrices:

$$\lambda_{jh}^{(w)} \sim \mathcal{N}(0, (\alpha_h^{(w)})^{-1}) \quad \text{for } j = 1, \dots, p_w,$$

with $\alpha_h^{(w)} \sim Ga(a_0, b_0)$,

for $w = 1, \dots, m$ and $h = 1, \dots, k$. This prior assumes the entire column shares the same precision parameter, and the precision $\alpha_h^{(w)}$ is assumed to follow a Gamma distribution $Ga(a_0, b_0)$. By giving the hyperparameter a_0 and b_0 small values (e.g., $a_0 = b_0 = 10^{-4}$), we get a uniform prior on the logarithmic scale for the precision parameter. This prior allows the posterior probability of the $\alpha_h^{(w)}$ parameters to concentrate at large values, achieving column-wise shrinkage (Tipping, 2001). In classical statistics, we induce column-wise shrinkage by adding a penalty term on $\mathbf{\Lambda}^{(w)}$. Commonly used penalties include mixed matrix norms: an L_1 norm penalizes each column, and either L_2 or L_∞ norms penalize the elements in that column:

$$\phi(\mathbf{\Lambda}^{(w)}) = \sum_{h=1}^k \|\boldsymbol{\lambda}_h^{(w)}\|_2 \quad \text{or} \quad \phi(\mathbf{\Lambda}^{(w)}) = \sum_{h=1}^k \|\boldsymbol{\lambda}_h^{(w)}\|_\infty.$$

In this framework, the L_1 norm penalty on columns achieves column-wise shrinkage.

These two approaches allow GFA models to capture covariance uniquely shared among arbitrary subsets of the observations and avoid modeling shared covariance in subsets that

are not maximally defined. But neither the ARD approach nor the mixed matrix norm penalties encourages element-wise shrinkage within loading columns. Adding element-wise sparsity is important because it results in interpretable and meaningful latent factors as shown in the sparse factor analysis research (West, 2003; Carvalho et al., 2008). One can either use Bayesian shrinkage on individual loadings (Carvalho et al., 2010) or mixed matrix norm with L_1 type penalties on each element (i.e., $\sum_{h=1}^k \sum_{j=1}^p |\lambda_{jh}^{(w)}|$). But these approaches still do not go far enough—the structure in the factor model is ignored. The main contribution of this study is to define a carefully structured Bayesian shrinkage prior on the loading matrix that encourages both element-wise shrinkage and also has non-parametric column-wise selection behavior for Bayesian GFA.

3. Bayesian Structured Sparsity

The column-wise sparse structure of \mathbf{A} in GFA models belongs to a general class of structured sparsity methods, which has drawn attention recently in the classical statistics literature (Zou and Hastie, 2005; Yuan and Lin, 2006; Jenatton et al., 2011, 2009; Kowalski, 2009; Kowalski and Torrsani, 2009; Zhao et al., 2009; Huang et al., 2011; Jia et al., 2010). For example, in structured sparse PCA, the loading matrix is constrained to have a set of specific patterns (Jenatton et al., 2009). Later Jenatton et al. (2011) and Huang et al. (2011) discussed more general structured variable selection methods in a regression framework. However, there has been little work in using Bayesian structured sparsity (with a few exceptions (Kyung et al., 2010; Engelhardt and Adams, 2014)). Starting from Bayesian shrinkage priors, we propose a structured hierarchical shrinkage prior that includes three levels of shrinkage, which is conceptually similar to tree structured shrinkage (Romberg et al., 2001), or global-local priors in the regression framework (Polson and Scott, 2010).

3.1 Bayesian Shrinkage Priors

Bayesian shrinkage priors have been widely used in latent factor models due to their non-parametric properties and interpretable solutions (West, 2003; Ghahramani et al., 2007; Carvalho et al., 2008; Polson and Scott, 2010; Knowles and Ghahramani, 2011; Bhattacharya and Dunson, 2011). In Bayesian statistics, a regularizing term, $\phi(\mathbf{A})$, may be viewed as a marginal prior proportional to $\exp(-\phi(\mathbf{A}))$; the regularized optimum then becomes a maximum a posteriori (MAP) solution (Polson and Scott, 2010). For example, the well known L_2 penalty for coefficients in linear regression models corresponds to Gaussian priors, also known as ridge regression or Tikhonov regularization (Hoerl and Kennard, 1970), whereas an L_1 penalty corresponds to double exponential priors or Laplace priors, also known as Bayesian Lasso (Tibshirani, 1996; Park and Casella, 2008; Hans, 2009).

When the goal of the regularization is to induce sparsity, the prior distribution should be chosen so that it has substantial probability mass around zero, which draws small effects toward zero, and heavy tails, which allows large signals to escape from substantial shrinkage (Carvalho et al., 2010; Armagan et al., 2011b). The canonical Bayesian sparsity-inducing prior is the spike-and-slab prior, which is a mixture of a point mass at zero and a flat distribution across the space of real values, often modelled as a Gaussian with a large variance term (West, 2003). The spike-and-slab prior has elegant interpretability by

estimating the probability that certain loadings are excluded, modeled by the ‘spike’ distribution, or included, modeled by the ‘slab’ distribution (Carvalho et al., 2008). This interpretability comes at the cost of having exponentially many possible configurations of the model inclusion parameters in the loading matrix.

Recently, scale mixtures of normal priors have been proposed as a computationally efficient alternative to the two component spike-and-slab prior (West, 1987; Carvalho et al., 2010; Polson and Scott, 2010; Armagan et al., 2011a,b; Bhattacharya et al., 2012): such priors generally assume normal distributions with a mixed variance term. The mixing distribution of the variance allows strong shrinkage near zero but weak regularization away from zero. For example, the inverse-gamma distribution on the variance term results in an ARD prior (Tipping, 2001), and an exponential distribution on the variance term results in a Laplace prior (Park and Casella, 2008). The horseshoe prior, with a half Cauchy distribution on the standard deviation as the mixing density, has become popular due to its strong shrinkage and heavy tail (Carvalho et al., 2010). A more general class of Beta mixtures of normals, called the three parameter Beta distribution, has been developed recently (Armagan et al., 2011b). Although these continuous shrinkage priors do not directly model the probability of feature inclusion, it has been shown in the regression framework that two layers of regularization (i.e., global regularization, across all coefficients, and local regularization, specific to each coefficient (Polson and Scott, 2010)) has behavior that is similar to the spike-and-slab prior in effectively modeling signal and noise separately, but enabling computational tractability (Carvalho et al., 2009). In this current study, we extend the Beta mixture of normals prior to three levels of hierarchy to induce desirable behaviors in the context of GFA models.

3.2 Three Parameter Beta Prior

For concreteness, the three parameter Beta (\mathcal{TPB}) distribution for a random variable $0 < Z < 1$ has the following density (Armagan et al., 2011b):

$$f(z; a, b, \nu) = \frac{\Gamma(a+b)}{\Gamma(a)\Gamma(b)} \nu^b z^{b-1} (1-z)^{a-1} \{1 + (\nu-1)z\}^{-(a+b)}, \quad (9)$$

where $a > 0, b > 0$ and $\phi > 0$. We denote this distribution as $\mathcal{TPB}(a, b, \nu)$. When $0 < a < 1$ and $0 < b < 1$, the distribution is bimodal, with two modes at 0 and 1. The *variance parameter* ν gives the distribution freedom: with fixed a and b , smaller values of ν put greater probability on $z = 1$, while larger values of ν move the probability mass towards $z = 0$ (Armagan et al., 2011b). With $\nu = 1$, this distribution is identical to a beta ($Be(b, a)$) distribution.

Let λ denote the parameter to which we are applying sparsity-inducing regularization. We assign the following \mathcal{TPB} normal scale mixture distribution, \mathcal{TPBN} , to λ :

$$\lambda | \varphi \sim \mathcal{N}\left(0, \frac{1}{\varphi} - 1\right), \quad \text{with} \quad \varphi \sim \mathcal{TPB}(a, b, \nu),$$

where the *shrinkage parameter* φ follows a \mathcal{TPB} distribution. With $a = b = 1/2$ and $\nu = 1$, this prior becomes the horseshoe prior (Carvalho et al., 2010; Armagan et al., 2011b; Gao et al., 2013). The bimodal property of φ induces two distinct shrinkage behaviors: the mode

near one encourages $\frac{1}{\varphi} - 1$ towards zero and induces strong shrinkage on λ ; the mode near zero encourages $\frac{1}{\varphi} - 1$ towards infinity and generates a diffuse prior. Further decreasing the variance parameter ν puts more support on stronger shrinkage (Armagan et al., 2011b; Gao et al., 2013). If we let $\theta = \frac{1}{\varphi} - 1$, then this mixture has the following hierarchical representation:

$$\lambda \sim \mathcal{N}(0, \theta), \quad \theta \sim Ga(a, \delta), \quad \delta \sim Ga(b, \nu).$$

3.3 Global-Factor-Local Shrinkage

The flexible representation of the \mathcal{TPB} prior makes it an ideal choice for latent factor models. In particular, one may induce sparsity in the loading matrix by assigning each element of the loading matrix an independent \mathcal{TPB} prior to encourage element-wise sparsity. However, local shrinkage does not allow the level of shrinkage to borrow strength across components of the factor matrix, nor does it enable non-parametric behavior of the model. Gao et al. (2013) extended the \mathcal{TPB} prior to three levels of hierarchical regularization on a loading matrix:

$$\begin{aligned} \varrho &\sim \mathcal{TPB}(e, f, \nu), && \text{Global} \\ \zeta_h &\sim \mathcal{TPB}\left(c, d, \frac{1}{\varrho} - 1\right), && \text{Factor-specific} \\ \varphi_{jh} &\sim \mathcal{TPB}\left(a, b, \frac{1}{\zeta_h} - 1\right), && \text{Local} \\ \lambda_{jh} &\sim \mathcal{N}\left(0, \frac{1}{\varphi_{jh}} - 1\right). \end{aligned} \tag{10}$$

At each of the three levels, a \mathcal{TPB} distribution is used to induce shrinkage with its own variance parameter (ν in Equation (9)), which has a further \mathcal{TPB} distribution depending on previous hierarchy. Specifically, the global shrinkage parameter ϱ applies strong shrinkage across all columns of the loading matrix, and jointly adjusts the support of ζ_h at either zero or one. This can be interpreted as inducing sufficient shrinkage across loading columns to identify the number of factors supported by the observed data. In particular, when ζ_h is close to one, all loadings in the column are zero, inducing column-wise shrinkage. The factor-specific regularization parameter, ζ_h , adjusts the shrinkage applied to each element of the h^{th} loading column, estimating the column-wise shrinkage by borrowing strength across all elements in that column. The local shrinkage parameter, φ_{jh} , creates element-wise sparsity in the loading matrix through a \mathcal{TPBN} . Three levels of shrinkage allow us to model both column-wise and element-wise shrinkage simultaneously, and give us non-parametric behavior in the number of factors.

Equivalently, this global-factor-local shrinkage prior can be written as:

$$\begin{aligned} \text{Global} & \begin{cases} \gamma \sim Ga(f, \nu), \\ \eta \sim Ga(e, \gamma), \end{cases} \\ \text{Factor-specific} & \begin{cases} \tau_h \sim Ga(d, \eta), \\ \phi_h \sim Ga(c, \tau_h), \end{cases} \end{aligned}$$

$$\text{Local} \quad \begin{cases} \delta_{jh} \sim \text{Ga}(b, \phi_h), \\ \theta_{jh} \sim \text{Ga}(a, \delta_{jh}), \end{cases} \\ \lambda_{jh} \sim \mathcal{N}(0, \theta_{jh}). \quad (11)$$

We further extend our prior to jointly model sparse and dense components by assigning to the local shrinkage parameter a two-component mixture distribution (Gao et al., 2013):

$$\theta_{jh} \sim \pi \text{Ga}(a, \delta_{jh}) + (1 - \pi) \delta(\phi_h), \quad (12)$$

where $\delta(\cdot)$ is the Dirac delta function. The motivation is that, in real applications such as the analysis of gene expression data, it has been shown that much of the variation in the observation is due to technical (e.g., batch) or biological effects (e.g., sex, ethnicity), which impact a large number of features (Leek et al., 2010). Therefore, the loadings corresponding to these effects will not be sparse. Equation (12) allows the local sparsity on the loading in Equation (10) to select between element-wise sparsity or column-wise sparsity, which induces a vector with a shared variance term: $\lambda_{jh} \sim \mathcal{N}\left(0, \frac{1}{\zeta_h} - 1\right)$. Modeling each element of a loading column from the same column-wise distribution has two possible outcomes: i) ζ_h in Equation (10) is close to 1 and the entire column is shrunk towards zero, effectively removing this factor; ii) ζ_h is close to zero, and all elements of the column have a shared Gaussian distribution, inducing only non-zero elements in that loading. We call included factors that have only non-zero elements *dense factors*. Jointly modeling sparse and dense factors effectively controls for the confounders' effects on the observation. We introduce indicator variables z_h , $h = 1, \dots, k$, to capture whether the component is sparse ($z_h = 1$) or either dense or removed ($z_h = 0$), and let $\mathbf{z} = [z_1, \dots, z_k]$. We put a Bernoulli distribution with parameter π on z_h and let π have a flat Beta distribution $Be(1, 1)$.

In the context of the GFA model, we put the global-factor-local \mathcal{TPB} priors independently on each loading matrix corresponding to w^{th} observation, $\mathbf{\Lambda}^{(w)}$. Let $\mathbf{Z} = [\mathbf{z}^{(1)}; \dots; \mathbf{z}^{(m)}] \in \mathbb{R}^{m \times k}$. Then $z_h^{(w)} = 1$ indicates that the h^{th} factor is active for observation w , and that only a sparse number of features from that observation load onto the corresponding factor. When $z_h^{(w)} = 0$, then either the h^{th} factor has a dense loading column for observation w , or the loading column is 0 for observation w . A zero loading column for observation w effectively decouples the factor from that observation, leading to the column-wise sparse behavior in previous GFA models (Virtanen et al., 2011). In our model, factors that have only zero loading columns across all observations are removed from the model.

4. Bayesian GFA Model Summary

We summarize our Bayesian GFA (BGFA) model as follows. The generative model for m coupled observations $\mathbf{y}_i^{(w)}$ with $w = 1, \dots, m$ and $i = 1, \dots, n$ is

$$\mathbf{y}_i^{(w)} = \mathbf{\Lambda}^{(w)} \mathbf{x}_i + \boldsymbol{\epsilon}_i^{(w)}, \quad \text{for } w = 1, \dots, m.$$

We re-write this BGFA model as a factor model by concatenating the m feature vectors for sample i into vector \mathbf{y}_i

$$\mathbf{y}_i = \mathbf{\Lambda} \mathbf{x}_i + \boldsymbol{\epsilon}_i,$$

$$\begin{aligned}\mathbf{x}_i &\sim \mathcal{N}_k(0, \mathbf{I}_k), \\ \boldsymbol{\epsilon}_i &\sim \mathcal{N}_p(0, \boldsymbol{\Sigma}),\end{aligned}\tag{13}$$

where $\boldsymbol{\Sigma} = \text{diag}(\sigma_1^2, \dots, \sigma_p^2)$. We put independent global-factor-local \mathcal{TPB} prior in Equation (11) on $\boldsymbol{\Lambda}^{(w)}$:

$$\begin{aligned}\text{Global} &\quad \begin{cases} \gamma^{(w)} \sim Ga(f, \nu), \\ \eta^{(w)} \sim Ga(e, \gamma^{(w)}), \end{cases} \\ \text{Factor-specific} &\quad \begin{cases} \tau_h^{(w)} \sim Ga(d, \eta^{(w)}), \\ \phi_h^{(w)} \sim Ga(c, \tau_h^{(w)}), \end{cases} \\ \text{Local} &\quad \begin{cases} \delta_{jh}^{(w)} \sim Ga(b, \phi_h^{(w)}), \\ \theta_{jh}^{(w)} \sim Ga(a, \delta_{jh}^{(w)}), \end{cases} \\ &\quad \lambda_{jh}^{(w)} \sim \mathcal{N}(0, \theta_{jh}^{(w)}).\end{aligned}$$

and allow local shrinkage to follow a two-component mixture

$$\theta_{jh}^{(w)} \sim \pi^{(w)} Ga(a, \delta_{jh}^{(w)}) + (1 - \pi^{(w)}) \delta(\phi_h^{(w)}),$$

where the mixture proportion follows a Beta distribution

$$\pi^{(w)} \sim Be(1, 1).$$

We put a conjugate inverse gamma distribution on the variances of the errors

$$\sigma_j^{-2} \sim Ga(a_\sigma, b_\sigma).$$

In our application of this model, we set the hyperparameters of the global-factor-local \mathcal{TPB} prior to $a = b = c = d = e = f = 0.5$, which recapitulates the horseshoe prior at all three levels of the hierarchy. The hyperparameters for the error variances, a_σ and b_σ , are set to 1 and 0.3 respectively to allow a relatively wide support of variances (Bhattacharya and Dunson, 2011). When there are only two coupled observations, the BGFA model simplifies to a BCCA model. In following sections we use BGFA to denote our model regardless of the number of observations.

5. Parameter Estimation

For posterior inference, we develop a variational expectation maximization (EM) algorithm to find a *maximum a posteriori* (MAP) estimate of model parameters (Dempster et al., 1977). In the maximization step, the loading columns specific to each observation are estimated jointly; this blocked approach has faster convergence than estimating each loading separately. In addition, we derived a Markov chain Monte Carlo (MCMC) algorithm that uses Gibbs sampling. MCMC also uses block updating of the loading matrix for faster mixing behavior (Bhattacharya and Dunson, 2011). In practice, when the data size allows, we first run a small number of MCMC iterations and use the last parameter sample as the starting parameter values for the variational EM algorithm (i.e., a warm start) (Andrieu et al., 2003). This hybrid approach encourages robustness of the variational EM algorithm to the starting point. Full details of parameter estimation methods are in Appendices A and B.

5.1 Identifiability

The standard latent factor model in Equation (1) is unidentifiable up to orthonormal rotation: for any orthogonal matrix \mathbf{P} with $\mathbf{P}^T \mathbf{P} = \mathbf{I}$, the new model with $\mathbf{\Lambda}' = \mathbf{\Lambda} \mathbf{P}^T$ and $\mathbf{x}' = \mathbf{P} \mathbf{x}$ produces the same covariance matrix with an identical likelihood. One traditional solution is to restrict the loading matrix to be lower-triangular (West, 2003; Carvalho et al., 2008). This solution gives a special role to the first k features in \mathbf{y} , and therefore the ordering of the features should be selected carefully (Carvalho et al., 2008).

Our BGFA model has equivalent unidentifiability: when we right multiply the combined loading matrix by \mathbf{P}^T and left multiply \mathbf{x} by \mathbf{P} we have an identical covariance matrix and likelihood. However, the structured shrinkage prior on BGFA puts additional constraints on the combined loading matrix by either favoring sparsity within a column ($z_h^{(w)} = 1$) or regarding the column as dense or zero ($z_h^{(w)} = 0$) for a specific observation. Any orthogonal transformation violating such desirable structure in the loading matrix, though resulting same likelihood, will have a low probability according to the prior and therefore a lower posterior probability than the original solution. We find that in practice this model is able to recover a structured loading matrix when there is sufficient sparsity in the true solution.

Our model does not specifically address label switching or sign invariance, but both of these identifiability problems are addressed more trivially after parameters are estimated. Label switching identifiability in these latent factor models has been studied in the context of mixture models (Stephens, 2000); the label switching problem implies that model averaging, either through averaging posterior samples of MCMC or averaging over point estimates from direct approaches, produces uninterpretable results. We addressed the sign and label switching invariances in our simulation studies as follows. After the MAP parameter estimate was found, we re-arranged the loadings to most closely match the simulated loadings, and we flipped the sign of the estimated loadings if they did not match the simulated ones. We performed this parameter cleaning across all of the methods considered in our simulation study. Furthermore, when we used BGFA for applications that were not sensitive to label switching or sign, such as covariance matrix estimation or identifying nonzero elements in sparse loadings, we did not modify the results of the loading matrix.

6. Simulations and Comparisons

We demonstrate the performance of our model on simulated data with both paired observations and multiple coupled observations.

6.1 Simulations for Paired Observations

We simulated two data sets with $p_1 = 100$, $p_2 = 120$ in order to compare related methods in the context of two paired observations. The number of samples in these simulations was $n = \{20, 30, 40, 50\}$. The number of samples was chosen to be smaller than both p_1 and p_2 to reflect the large p , small n problem, which is ubiquitous in genomics applications (West, 2003) and motivates our structured approach. We first simulated observations with only sparse latent factors (*Sim1*). In particular, we set $k = 6$, where two sparse factors are shared by both observations (factor 1 and 2; in Table 1), two sparse factors are specific to $\mathbf{y}^{(1)}$ (factor 3 and 4; Table 1), and two sparse factors are specific to $\mathbf{y}^{(2)}$ (factor 5 and

Factors	1	2	3	4	5	6
$\mathbf{Y}^{(1)}$	S	S	S	S	0	0
$\mathbf{Y}^{(2)}$	S	S	0	0	S	S

Table 1: **Six latent factors in *Sim1* with two observation matrices.** S represents a sparse vector; 0 represents a zero vector.

Factors	1	2	3	4	5	6	7	8
$\mathbf{Y}^{(1)}$	S	D	S	S	D	0	0	0
$\mathbf{Y}^{(2)}$	S	D	0	0	0	S	S	D

Table 2: **Eight latent factors in *Sim2* with two observation matrices.** S represents a sparse vector; D represents a dense vector; 0 represents a zero vector.

6; Table 1). The elements in the sparse loading matrix were randomly generated from a $\mathcal{N}(0, 4)$ Gaussian distribution, and sparsity was induced by setting 90% of the elements in each loading column to zero at random (Figure 2A). Latent factors \mathbf{x} were generated from $\mathcal{N}_6(0, \mathbf{I}_6)$. Residual error was generated by first generating the $p = p_1 + p_2$ diagonals on the residual covariance matrix Σ from a uniform distribution on $(0.5, 1.5)$, and then generating each column of the error matrix from $\mathcal{N}_p(\mathbf{0}, \Sigma)$.

We performed a second simulation that included both sparse and dense latent factors (*Sim2*). In particular, we extended *Sim1* to $k = 8$ latent factors, where one of the shared sparse factors is now dense, and two dense factors, each specific to one observation, were added. For all dense factors, each loading was generated according to a $\mathcal{N}(0, 4)$ Gaussian distribution (Table 2; Figure 2C).

6.2 Simulations for Multiple Observations

To compare different methods in the context of multiple observations, we performed two additional simulations (*Sim3* and *Sim4*) on four data sets with $p_1 = 70$, $p_2 = 60$, $p_3 = 50$ and $p_4 = 40$. The number of samples, as above, was set to $n = \{20, 30, 40, 50\}$. In *Sim3*, and we let $k = 6$ and only simulated sparse factors: the first three factors were specific to $\mathbf{y}^{(1)}$, $\mathbf{y}^{(2)}$ and $\mathbf{y}^{(3)}$ respectively, and last three corresponded to different subsets of the observations (Figure 3A; Table 3). In *Sim4* we let $k = 8$, and, as with *Sim2*, included both sparse and dense factors (Figure 3B; Table 4). Observations in these two simulations were generated following the same method as in the simulations with two observations.

6.3 Methods for Comparison

We compared our BGFA model with three available CCA approaches: the Bayesian CCA model with an ARD prior (BCCA-ARD) (Klami et al., 2013), a regularized version of CCA (RCCA) (Gonzalez et al., 2008) and sparse CCA (SCCA) (Witten and Tibshirani, 2009).

The Bayesian CCA model studied by Klami et al. (2013) puts an ARD prior on each column of the loading matrices, encouraging column-wise shrinkage of the loading matrix but not sparsity within these loadings. The extension of BCCA-ARD allows multiple coupled

Factors	1	2	3	4	5	6
$\mathbf{Y}^{(1)}$	S	0	0	S	0	0
$\mathbf{Y}^{(2)}$	0	S	0	S	S	S
$\mathbf{Y}^{(3)}$	0	0	S	0	S	S
$\mathbf{Y}^{(4)}$	0	0	0	0	0	S

Table 3: **Six latent factors in *Sim3* with four observation matrices.** *S* represents a sparse vector; 0 represents a zero vector.

Factors	1	2	3	4	5	6	7	8
$\mathbf{Y}^{(1)}$	S	0	0	0	D	0	0	0
$\mathbf{Y}^{(2)}$	0	S	0	S	0	D	0	0
$\mathbf{Y}^{(3)}$	0	0	S	S	0	0	D	0
$\mathbf{Y}^{(4)}$	0	0	S	0	0	0	0	D

Table 4: **Eight latent factors in *Sim4* with four observation matrices.** *S* represents a sparse vector; *D* represents a dense vector; 0 represents a zero vector.

observations. In our simulations, we ran the BCCA-ARD model with the factor number set to the correct values: $k = 6$ in *Sim1* and *Sim3*, $k = 8$ in *Sim2* and *Sim4*.

We ran the regularized version of classical CCA (RCCA) for comparison in *Sim1* and *Sim2* (Gonzalez et al., 2008). Classical CCA aims to find k canonical projection directions \mathbf{u}_h and \mathbf{v}_h ($h = 1, \dots, k$) for $\mathbf{Y}^{(1)}$ and $\mathbf{Y}^{(2)}$ respectively such that i) the correlation between $\mathbf{u}_h^T \mathbf{Y}^{(1)}$ and $\mathbf{v}_h^T \mathbf{Y}^{(2)}$ is maximized for $h = 1, \dots, k$; and ii) $\mathbf{u}_h^T \mathbf{Y}^{(1)}$ is orthogonal to $\mathbf{u}_{h'}^T \mathbf{Y}^{(1)}$ with $h' \neq h$, and similarly for \mathbf{v}_h and $\mathbf{Y}^{(2)}$. Let these two projection matrices be denoted $\mathbf{U} = [\mathbf{u}_1, \dots, \mathbf{u}_k] \in \mathbb{R}^{p_1 \times k}$ and $\mathbf{V} = [\mathbf{v}_1, \dots, \mathbf{v}_k] \in \mathbb{R}^{p_2 \times k}$. These matrices are the maximum likelihood estimates of the shared loading matrices in the Bayesian CCA model up to orthogonal transformations (Bach and Jordan, 2005). However, classical CCA requires the observation covariance matrices to be non-singular and thus is not applicable in the current simulations, where $n < p_1, p_2$. Therefore, we used a regularized version of CCA (RCCA) (Gonzalez et al., 2008) by adding $\lambda_1 \mathbf{I}_{p_1}$ and $\lambda_2 \mathbf{I}_{p_2}$ to the two sample covariance matrices. The two regularization parameters λ_1 and λ_2 were chosen according to leave-one-out cross-validation with the search space defined on a 11×11 grid from 0.0001 to 0.01. The projection directions \mathbf{U} and \mathbf{V} were estimated using the best regularization parameters. We let $\mathbf{P}' = [\mathbf{U}; \mathbf{V}]$; this matrix was comparable to the simulated loading matrix up to orthogonal transformations. We calculated the matrix \mathbf{P} such that the Frobenius norm between $\mathbf{\Lambda}' \mathbf{P}'^T$ and simulated $\mathbf{\Lambda}$ was minimized, with the constraint that $\mathbf{P}'^T \mathbf{P}' = \mathbf{I}$, possible because of the constraint preserving updates of the objective function (Wen and Yin, 2013). After finding the optimal orthogonal transformation matrix, we recovered $\mathbf{\Lambda}' \mathbf{P}'^T$ as the estimated loading matrix. We chose $k = 6$ and $k = 8$ regularized projections for comparison in *Sim1* and *Sim2* respectively, the true number of latent linear factors. RCCA does not naively apply to multiple coupled observations, and thus was not applied to *Sim3* or *Sim4*.

The sparse CCA (SCCA) method (Witten and Tibshirani, 2009) maximizes correlation between two observations after projecting the original space with a sparsity-inducing penalty

onto the projection directions, producing sparse matrices \mathbf{U} and \mathbf{V} . This method is encoded in the R package PMA (Witten et al., 2013). For *Sim1* and *Sim2*, as with RCCA, we found an optimal orthogonal transformation matrix \mathbf{P} such that the Frobenius norm between $\mathbf{\Lambda}'\mathbf{P}^T$ and simulated $\mathbf{\Lambda}$ was minimized, where $\mathbf{\Lambda}'$ was the vertical concatenation of the recovered sparse \mathbf{U} and \mathbf{V} . We chose $k = 6$ and $k = 8$ sparse projections in *Sim1* and *Sim2*, respectively, representing the true number of latent factors. An extension of SCCA allows for multiple observations (Witten and Tibshirani, 2009). For *Sim3* and *Sim4*, we recovered four sparse projection matrices $\mathbf{U}^{(1)}, \mathbf{U}^{(2)}, \mathbf{U}^{(3)}, \mathbf{U}^{(4)}$ and set $\mathbf{\Lambda}'$ as the vertical concatenation of the four matrices. Then the orthogonal transformation matrix \mathbf{P} was calculated similarly by minimizing the Frobenius norm between $\mathbf{\Lambda}'\mathbf{P}^T$ and the true loading matrix $\mathbf{\Lambda}$. The number of canonical projections was set to $k = 6$ in *Sim3* and $k = 8$ in *Sim4*, again corresponding to the true number of latent factors.

6.4 Metrics for Comparison

To quantitatively compare the results from applying BGFA with the alternative methods, we used the sparse and dense stability indices proposed in our previous study (Gao et al., 2013) to compare the simulated matrices with the recovered matrices. The sparse stability index (SSI) measures the similarity between columns of sparse matrices. SSI is invariant to column scale and label switching, but it penalizes factor splitting and matrix rotation; larger values of the SSI indicate better recovery. The dense stability index (DSI) quantifies the difference between dense matrix columns, and is invariant to orthogonal matrix rotation, label switching, and scale; DSI values closer to zero indicate better recovery. We extended the stability indices to allow multiple coupled matrices as in the current simulations. In *Sim1* and *Sim3*, all factors were regarded as sparse, and SSIs were calculated between true *combined* loading matrices and combined recovered loading matrices. In *Sim2* and *Sim4*, because none of the compared methods explicitly distinguished sparse and dense factors, we categorized them as follows. We first selected a global sparsity threshold on the elements of the combined loading matrix; here we set that value to 0.15. Elements below this threshold were set to zero in the loading matrix. Then we chose the first five loading columns with the fewest non-zero elements as the sparse loadings in *Sim2* and the first four loadings with the fewest non-zero elements as the sparse loadings in *Sim4*. The remaining loading columns were considered dense loadings. We found that varying the sparsity threshold did not affect the separation of sparse and dense loadings significantly. SSIs were then calculated for the true combined sparse loading matrix and the combined recovered sparse loadings. To calculate DSIs, we treated the loading matrices $\mathbf{\Lambda}^{(w)}$ for each observation m separately, and calculated the DSI for the recovered dense components of each observation. The final DSI for each method was the sum of the m separate DSIs.

6.5 Results of the Comparison

We first evaluated the performance of our model in terms of recovering the correct number of sparse and dense factors in the four simulations. We set the number of MCMC iterations to 50 and ran our model 20 times from random starting points. In *Sim1* and *Sim3*, we set the starting number of factors to 10. Our BGFA model identified the correct number of sparse latent factors in 17 out of 20 runs (85%) in *Sim1* (Figure 2B), and 18 out of 20 runs

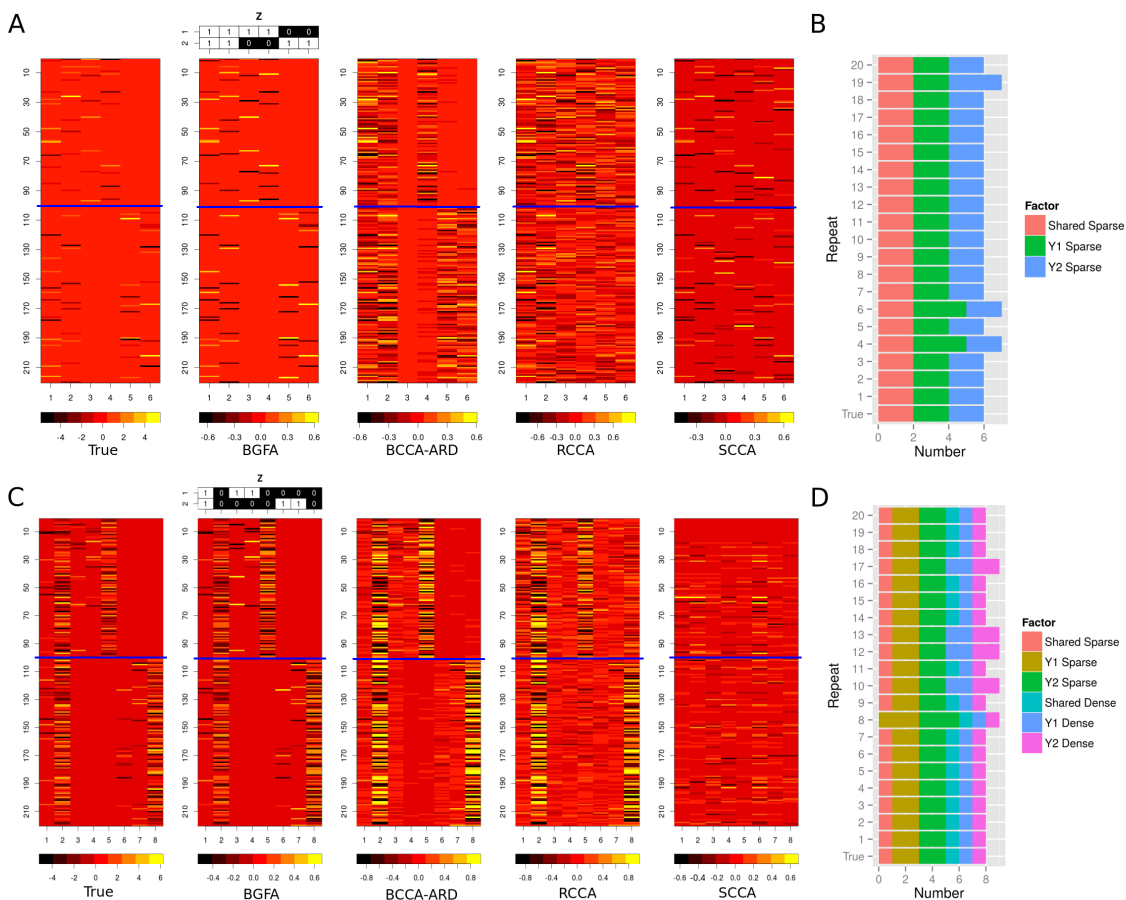


Figure 2: **Simulation results with two paired observations with $n = 40$.** We re-ordered the columns of the recovered matrices and, where necessary, multiplied a column by -1 for easier visual comparisons. Panel A: Comparison of recovered loading matrices using different models on *Sim1*. Panel B: Recovered factors across 20 random restarts of BGFA for *Sim1*. Panel C: Comparison of recovered loading matrices using different models on *Sim2*. Panel D: Recovered factors across 20 random restarts of BGFA for *Sim2*.

(90%) in *Sim3* (Figure 3B). In *Sim2* and *Sim4*, we set the starting factor number to 15. Our BGFA model identified the correct number of sparse latent factors in 15 out of 20 runs (75%) in *Sim2* (Figure 2D), and 19 out of 20 runs (95%) in *Sim4* (Figure 3D).

We ran the other methods on the four simulations and compared our results against those from BGFA. Our BGFA model recovered the closest matches to the simulated loading matrices across the compared methods from a visual inspection (Figures 2 and 3). We then quantitatively compared results using the two stability indices. Our model produced the best SSIs among the methods across the different sample sizes in *Sim1* and *Sim3* for the recovered sparse factors (Figures 4A and 5A). The performance of BCCA-ARD and BGFA-ARD was limited in the two sparse simulations because the ARD prior does not produce sufficient element-wise sparsity within a loading column (Figure 2A and 3A), resulting in poor SSIs (Figures 4A and 5A). RCCA also suffered in *Sim1* because the recovered

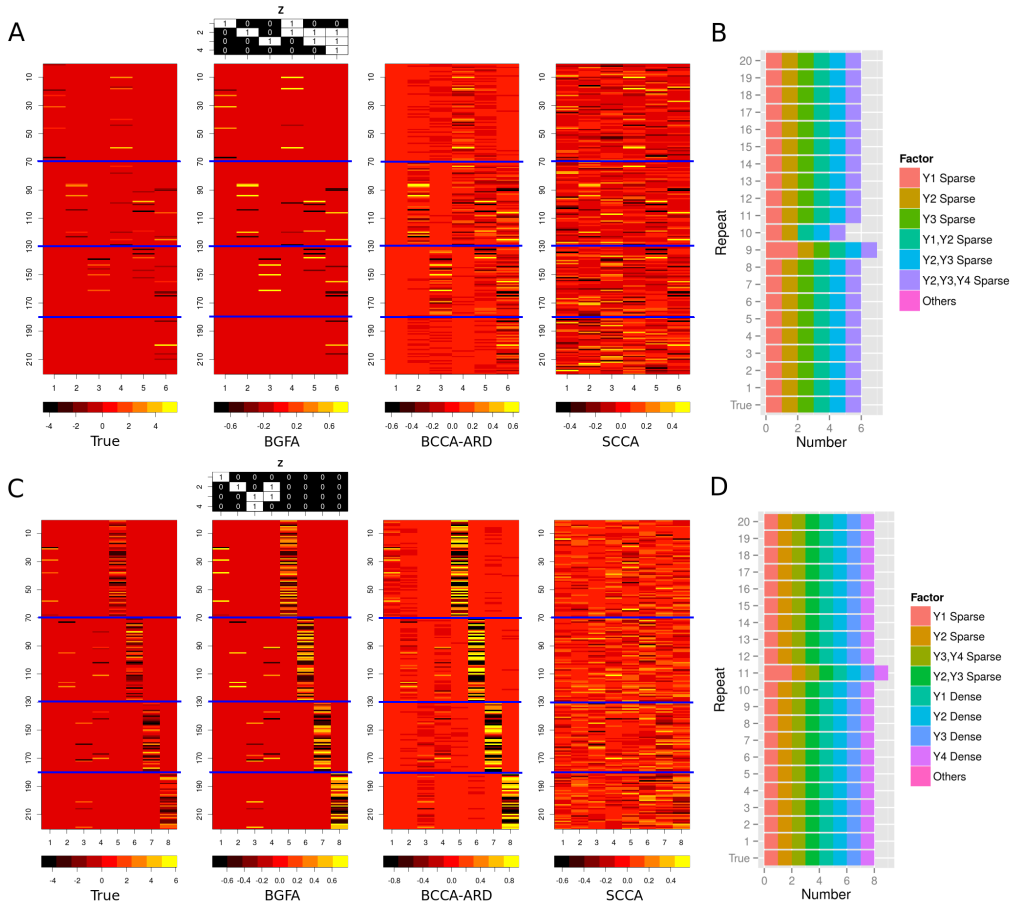


Figure 3: **Simulation results with four observation matrices with $n = 40$.** We reordered the columns of the recovered matrices and, where necessary, multiplied a column by -1 for easier visual comparisons. Panel A: Comparison of recovered loading matrices using different models on *Sim3*. Panel B: Recovered factors across 20 random restarts of BGFA in *Sim3*. Panel C: Comparison of recovered loading matrices using different models on *Sim4*. Panel D: Recovered factors across 20 random restarts of BGFA on *Sim4*.

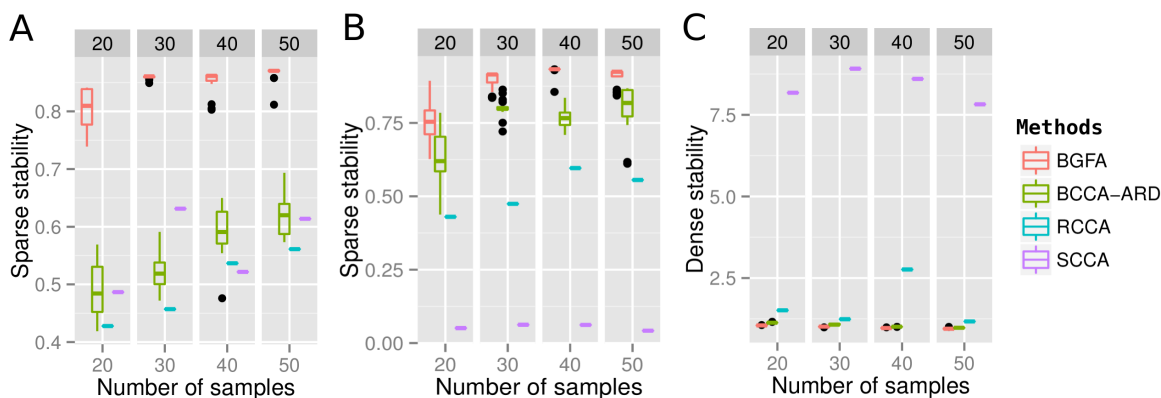


Figure 4: **Comparison of stability indices on recovered loading matrices with two observations.** For SSI, a larger value indicates better recovery; for DSI, a smaller value indicates better recovery. Panel A: Comparison of SSI across four methods and four sample sizes on *Sim1*. Panel B: Comparison of SSI across the sparse loadings from four methods and four sample sizes on *Sim2*. Panel C: Comparison of DSI across the dense loadings from four methods and four sample sizes on *Sim2*.

loadings were not sufficiently sparse (Figure 2A), resulting in poor SSIs (Figure 4A). SCCA recovered shared sparse loadings well in *Sim1* (Figure 2A). However SCCA does not model local covariance structure, and therefore was unable to recover the sparse loadings specific to subsets of observations in *Sim1* and *Sim3* (Figures 2A and 3A), resulting again in poor SSIs (Figure 4A and 5A).

Adding dense components in *Sim2* and *Sim4* did not deteriorate the sparse results from our BGFA model: BGFA effectively identified both sparse and dense factors (Figures 2C and 3C). Results from BGFA had the best SSIs and DSIs among the compared methods across all sample sizes (Figures 4B, 4C, 5B, and 5C). BCCA-ARD did not recover matrices with sparsity matching that found in the simulations (Figures 2C and 3C), which resulted in SSIs worse than the SSIs for BGFA (Figures 4B and 5B). As a consequence of not matching sparse loadings well, BCCA-ARD had difficulty recovering dense loadings (Figures 4C and 5C). For the SCCA method, both sparse loading recovery and dense loading recovery deteriorated substantially when the dense factors were included (Figures 2C and 3C), as reflected in both the SSIs and DSIs (Figures 4B, 4C, 5B, and 5C).

7. Real Data Applications

7.1 Exposure Gene Expression Data Analysis

We applied our model to gene expression data from the Cholesterol and Pharmacogenomic (CAP) study, consisting of expression level measurements for 10,195 genes in 480 lymphoblastoid cell lines (LCLs) after 24-hour exposure to either a control buffer ($\mathbf{Y}^{(1)}$) or 2 μM simvastatin acid ($\mathbf{Y}^{(2)}$) (Mangravite et al., 2013; Brown et al., 2013). In this example, the two observations represent gene expression levels on the same samples and genes after the two different exposures. We projected the expression levels to the quantiles of

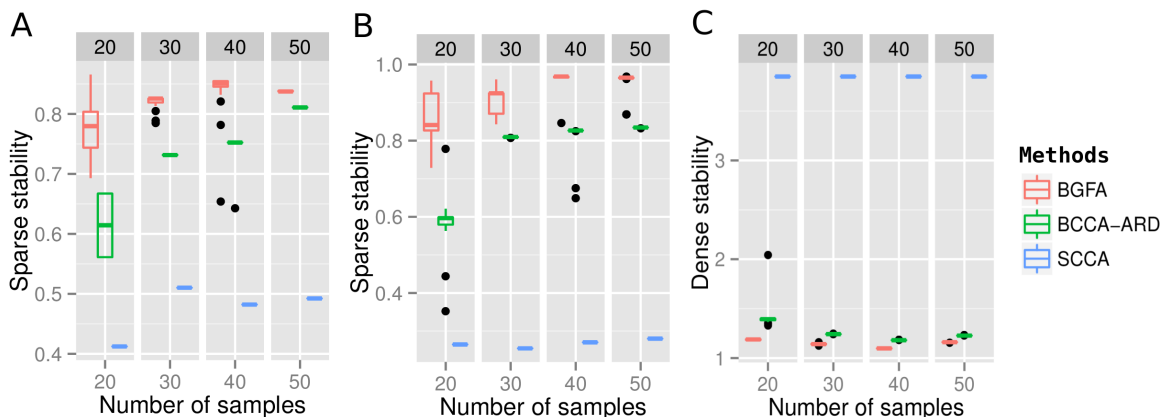


Figure 5: **Comparison of stability indices on recovered loading matrices with four observations.** For SSI, a larger value indicates better recovery; for DSI, a smaller value indicates better recovery. Panel A: Comparison of the SSI across three methods and four sample sizes on *Sim3*. Panel B: Comparison of SSIs across the sparse loadings from three methods and four sample sizes on *Sim4*. Panel C: Comparison of DSIs across the dense loadings from three methods and four sample sizes on *Sim4*.

	$\mathbf{Y}^{(1)}$	S	S	0	D	D	0	Rest	Total
	$\mathbf{Y}^{(2)}$	S	0	S	D	0	D		
#Factor	One run	19	221	217	6	35	31	7	536
	Average	23	175	200	5	26	28	16	473
PVE	Average	0.35%	0.42%	0.61%	3.63%	31.97%	38.91%	14.80%	90.67%

Table 5: **Recovered latent factors in the CAP gene expression data with two observation matrices.** S represents a sparse vector; D represents a dense vector; 0 represents a zero vector. PVE: proportion of variance explained.

a standard normal within gene and applied our BGFA model with the initial number of factors set to $k = 2000$. The large size of these data necessitated eliminating MCMC runs from the parameter estimation procedure, and we used EM with random initializations to estimate model parameters. We performed parameter estimation 100 times on these data. Across these 100 runs, the estimated number of recovered factors was approximately 473 (Supplemental Table S1).

We computed the proportion of variance explained (PVE) by each factor (Figure 6A). The PVE for the h^{th} factor was calculated as the variance explained by the h^{th} factor divided by the total variance: $tr(\boldsymbol{\lambda}_h \boldsymbol{\lambda}_h^T) / tr(\boldsymbol{\Lambda} \boldsymbol{\Lambda}^T + \boldsymbol{\Sigma})$. The first three $\mathbf{Y}^{(1)}$ specific dense factors explained 25.10% of the total variance, and the first three $\mathbf{Y}^{(2)}$ specific dense factors explained 31.23% of the total variance. We also found that 98.6% of the sparse factors contained fewer than 100 genes, and 0.31% of sparse factors had greater than 500 genes (Figure 6B).

The sparse factors specific to each observation characterize the local covariance estimates after controlling the observation matrices for the jointly modeled shared and specific

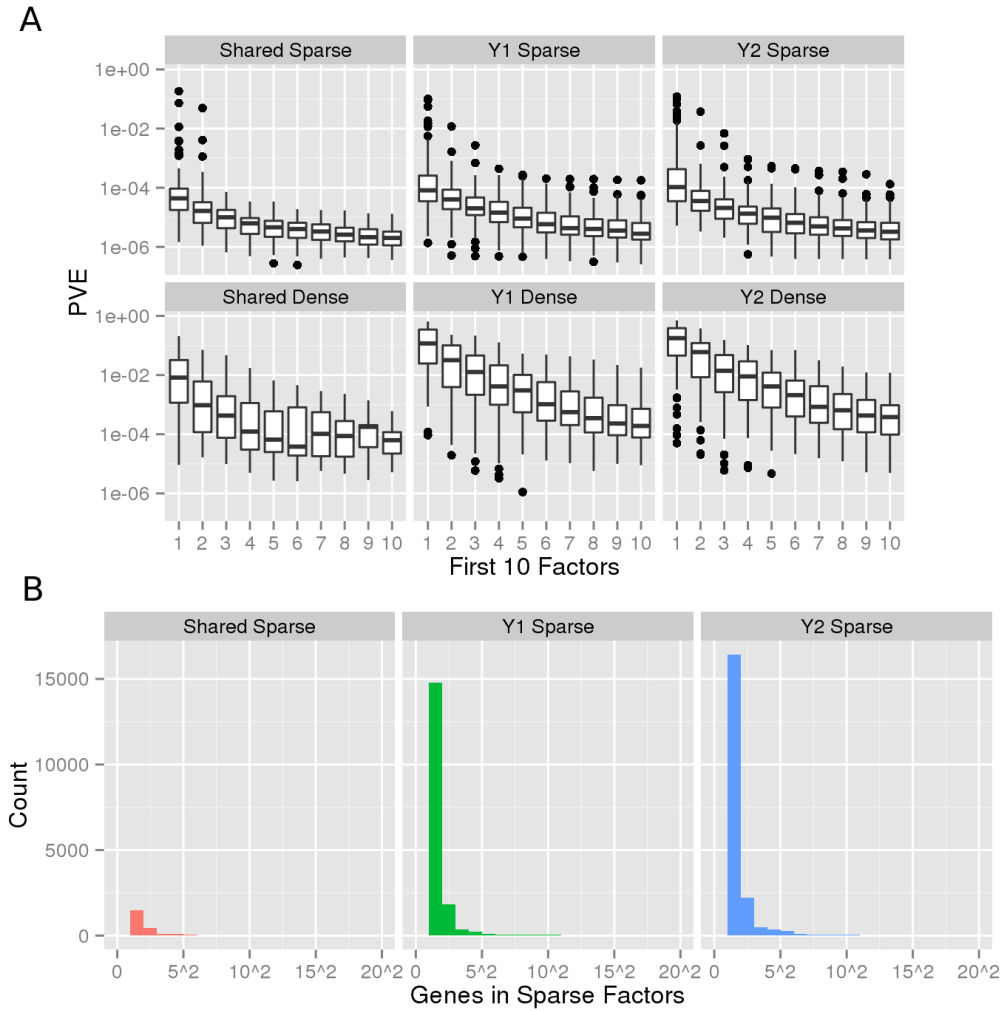


Figure 6: **Results of applying BGFA to the CAP gene expression data.** These figures represent the results over 100 runs of parameter estimation. $\mathbf{Y}^{(1)}$ denotes the observation from buffer-treated samples; $\mathbf{Y}^{(2)}$ denotes the observation from statin-treated samples. Panel A: the proportion of variance explained (PVE) by different factor types. Factors are ordered by their PVE's and first 10 factors are displayed. PVE is on the log₁₀ scale. Panel B: Histogram of the number of genes from different sparse factors. The count is displayed on the square root scale.

dense factors. Biologically, this has the effect of controlling for variation in gene expression levels due to ubiquitous technical and biological confounders such as batch effects or population structure among samples, which tend to affect many gene expression levels and hence have dense loadings (Gao et al., 2013). We chose a run with 536 factors to illustrate the gene clusters in the sparse factors. In this run, there were 221 sparse factors specific to $\mathbf{Y}^{(1)}$, 217 sparse factors specific to $\mathbf{Y}^{(2)}$, and 19 shared sparse factors (Table 5). We found that 289 (63.2%) of the sparse factors contained two well-correlated genes. We extracted the three largest sparse factor from the three sparse classes (i.e., shared and specific to each observation) and applied Gene Ontology (GO) enrichment analysis using DAVID software (Huang et al., 2009) to analyze the recovered gene clusters. The largest sparse factor specific to $\mathbf{Y}^{(1)}$, the buffer-treated observations, contained 478 genes. We found that 202 significantly enriched gene annotation terms were returned by DAVID ($p \geq 0.05$). The most significant annotation term was *phosphoprotein*, with 236 genes with this annotation in the sparse factor (52.5%; $p \leq 1.5 \times 10^{-10}$ based on a hypergeometric test) (Huang et al., 2009). The largest sparse factor specific to $\mathbf{Y}^{(2)}$, the statin-treated observations, contained 355 genes. For this factor, 138 significantly enriched gene annotation terms were identified at the same p-value threshold. The most significant annotation term was *nucleus*, with 140 genes having this annotation (41.4%; $p \leq 2.8 \times 10^{-15}$ based on a hypergeometric test). The largest sparse factor shared by both observations contained 24 genes. DAVID returned four annotation terms at the same p-value threshold. The most significant annotation term was *regulation of lymphocyte activation*, with three genes having this annotation ($p \leq 0.016$; hypergeometric test). Complete GO analysis results are in Supplementary Table S2.

7.1.1 OBSERVATION-SPECIFIC CO-EXPRESSION NETWORK RECONSTRUCTION

As we pursued more carefully elsewhere (Gao et al., 2014), the recovered sparse factors specific to a single observation may be used to construct a gene co-expression network that is uniquely found in that observation. We denote $\mathbf{B}_s^{(w)}$ as the sparse loadings in $\mathbf{B}^{(w)}$ ($w \in \{1, 2\}$). Then $\mathbf{\Omega}_s^{(w)} = \mathbf{B}_s^{(w)} \text{Var}(\mathbf{X}_s^{(w)}) (\mathbf{B}_s^{(w)})^T + \mathbf{\Sigma}^{(w)}$ represents the regularized estimate of the covariance matrix specific to each observation after controlling for the contributions of the dense factors. $\mathbf{X}_s^{(w)}$ are the factors corresponding to the sparse loadings for observation w . In our model, $\text{Var}(\mathbf{X}_s^{(w)}) = \mathbf{I}$, and so the covariance matrix specific to one of the two observations is written as $\mathbf{\Omega}_s^{(w)} = \mathbf{B}_s^{(w)} (\mathbf{B}_s^{(w)})^T + \mathbf{\Sigma}^{(w)}$. We inverted this estimate of the positive definite covariance matrix to get a precision matrix $\mathbf{R}^{(w)} = (\mathbf{\Omega}_s^{(w)})^{-1}$. The partial correlation between gene j_1 and j_2 is then calculated by normalizing the precision matrix (Edwards, 2000; Schfer and Strimmer, 2005):

$$\rho_{j_1 j_2}^{(w)} = - \frac{r_{j_1 j_2}^{(w)}}{\sqrt{r_{j_1 j_1}^{(w)} r_{j_2 j_2}^{(w)}}}.$$

A partial correlation that is zero for two genes suggests that they are conditionally independent (conditional on the remaining genes in the network); non-zero partial correlation implies a direct relationship between two genes. Thus, in the recovered network, each vertex is a gene and each edge is a non-zero entry between the pair of connected genes in the normalized precision matrix. The resulting undirected network induces a Gaussian Markov

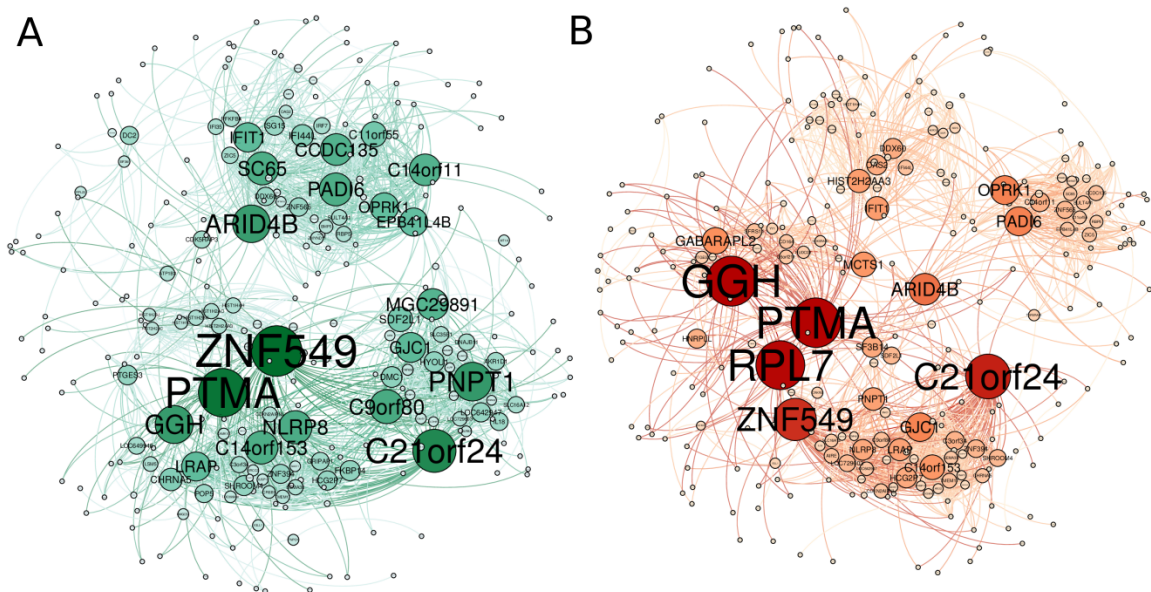


Figure 7: **Observation-specific gene co-expression networks from CAP data.** For each of the 100 EM runs, two networks were constructed. The node and label size is scaled according to the number of shortest paths from all vertices to all others that pass through that node (i.e., *betweenness centrality*).

random field, also known as a Gaussian graphical model (Edwards, 2000; Schfer and Strimmer, 2005; Koller and Friedman, 2009). We used GeneNet (Schfer and Strimmer, 2005) to compute the network from our estimates of the regularized covariance matrix.

We used following ensemble approach to combine the results from each of the 100 runs to construct a single observation-specific gene co-expression network for each observation. For each run, we constructed a network by connecting genes with partial correlation greater than a threshold (0.05). Then we combined the results from the 100 networks to construct a single network by keeping the edges that appeared in more than 10 (10%) of the single-run networks. The resulting two observation-specific gene co-expression networks contained 277 genes and 1,593 edges (buffer treated observation, Figure 7A), and 275 genes and 1,531 edges (statin-treated observation, Figure 7B).

7.2 Multi-trait multi-SNP association mapping

As a second application, we applied our model to HapMap phase 3 (HM3) project genotype and gene expression data to perform a multi-SNP multi-trait association mapping. The data consist of 1,335,434 single nucleotide polymorphisms (SNPs) across the genome and gene expression levels for 17,229 genes in 608 individuals (Stranger et al., 2012). SNPs are represented by $\{0, 1, 2\}$, representing the number of copies of the less frequent genetic variant (out of two total copies and two possible variants); gene expression levels are represented as a real number, which we quantile normalized as before Brown et al. (2013), although we did not correct for principal components. The SNP data were centered.

	$\mathbf{Y}^{(1)}$	D	0	0	0	S	0	
	$\mathbf{Y}^{(2)}$	0	D	0	D	0	S	
	$\mathbf{Y}^{(3)}$	0	0	D	D	0	0	
#Factor	One run	3	2	30	5	208	64	
	Average	3	10	26	4	537	68	
PVE	Average	45.13%	0.00%	12.22%	4.04%	11.36%	0.12%	
	$\mathbf{Y}^{(1)}$	0	0	S	S	S		
	$\mathbf{Y}^{(2)}$	0	S	S	0	S	Rest	Total
	$\mathbf{Y}^{(3)}$	S	S	0	S	S		
#Factor	One run	554	76	39	81	16	15	1,093
	Average	276	58	51	55	9	21	1,118
PVE	Average	0.50%	0.07%	1.42%	2.02%	0.05%	12.82%	89.65%

Table 6: **Recovered factors for HM3 data with three observations.** S represents a sparse vector; D represents a dense vector; 0 represents a zero vector. PVE: proportion of variance explained.

In standard eQTL studies, the methodology for finding eQTLs is to control for covariates and confounders in the gene expression data, and perform $p \times q$ univariate tests of association for p genes and q SNPs. These tests are performed using a linear regression model with gene expression levels for one gene across n individuals as the response and the genotypes of a single SNP across n individuals as the predictor (Stephens and Balding, 2009). While the univariate testing approach is simple, performing this association test jointly over multiple SNPs and multiple genes would have biological meaning and allow structure to be built into the model for the SNPs or genes (Engelhardt and Adams, 2014). In particular, *pleiotropic* SNPs are SNPs that regulate the levels of multiple genes simultaneously; conversely, *allelic heterogeneity* refers to traits (here, gene expression levels) that are regulated by multiple genetic variants. A multi-SNP, multi-trait model of association would allow the identification of pleiotropic SNPs and allelic heterogeneity, whereas univariate approaches do not warrant these interpretations (Zhang et al., 2010; Lee et al., 2012; Stephens, 2013; Brown et al., 2013).

In this application of BGFA, we chose chromosome 22 as a demonstration. After filtering SNPs with minor allele frequency (MAF) smaller than 0.05, we were left with 16,505 SNPs on chromosome 22 for the 608 individuals. We let the SNP data matrix be observation one ($\mathbf{Y}^{(1)}$). We let the gene expression level data for the genes on chromosome 22 (403 genes) be observation two ($\mathbf{Y}^{(2)}$), and we let the gene expression levels for the genes on all other autosomal chromosomes (16,826 genes) be observation three ($\mathbf{Y}^{(3)}$). We applied BGFA to these three observation matrices using the EM algorithm with the initial factor number set to $k = 2,000$; we repeated this process 100 times with random initializations. Across 100 runs, the estimated number of factors was approximately 1,118 (Supplemental Table S3). The sparse factors that were active in the SNP observation and also active in either or both of the two expression observations reflected multi-SNP multi-trait associations (Figure 8B). We chose a run with 1,093 factors to demonstrate the results of our model (Table 6).

We first analyzed the three SNP-specific dense factors. We found that these factors cluster individuals with shared ancestry, and specifically identify Mexicans (MEX), Gujarati Indians (GIH), and Maasai individuals (MKK) (Figure 8A). The population structure among the 608 individuals was captured well by these three dense factors, as has been demonstrated previously (Price et al., 2006; Novembre and Stephens, 2008; Engelhardt and Stephens, 2010). We next analyzed the sparse factors that were active in the SNP observation and also active in either or both of the two gene expression observations. Along with active SNP observations, there were 39 sparse factors that included the chromosome 22 gene expression levels, 81 sparse factors that included all other gene expression levels, and 16 sparse factors that included gene expression levels from all chromosomes (136 in total). For each SNP with a non-zero loading on one of those factors, we fitted a univariate linear regression model between this SNP and every gene that had non-zero loading on this same factor. The SNP was the predictor and gene expression level was the response. The p -values for all linear models SNP-gene pairs were calculated to quantify the strength of evidence for a non-zero coefficient (i.e., a linear association). For comparison, we randomly selected a gene from another factor every SNP-gene pair and calculated p -values by fitting a linear regression. The distribution of p -values for SNP-gene pairs in the same sparse loading column was substantially enriched for low p -values, suggesting that this approach identified meaningful associations (Figure 8C).

8. Discussion

In this study, we developed a Bayesian structured sparse prior for group factor analysis. The structured sparse prior is built using three hierarchical layers of the three parameter Beta (\mathcal{TPB}) distribution. The first layer controls global shrinkage; by adjusting global shrinkage, this layer allows the model to identify the number of factors non-parametrically. The second layer controls factor-specific shrinkage and adapts the levels of shrinkage on each loading column. The third layer controls local, element-wise shrinkage, and enables sparse factors that perform feature selection within each loading column. In addition, element-wise shrinkage may be avoided through a two component mixture model at this local shrinkage layer. This resulting model identifies factors that have both sparse and dense loadings. Allowing dense factors has important implications in real applications when the data are have confounding effects that require control. In the genomic applications here, they can be effectively used to capture and control confounding effects such as population structure and batch effects.

We extended the Bayesian structured sparse prior to Bayesian group factor analysis models (BGFA) with multiple coupled observations. When there are two paired observations, BGFA model simplifies to a BCCA model. Previous studies on BCCA and BGFA had relied on ARD priors for column-wise shrinkage (Virtanen et al., 2011; Klami et al., 2013) to decouple the latent space from certain observations. Our column-wise shrinkage resembles this behavior. In addition, our local shrinkage induces element-wise sparsity, allowing simpler representation of latent space to arbitrary subsets of observations.

Using simulations, we evaluated the loading matrices recovered by our BGFA model from simulated data with substantial structure. In most runs, BGFA identified the correct number of sparse and dense factors and the values of the loadings for those factors; related

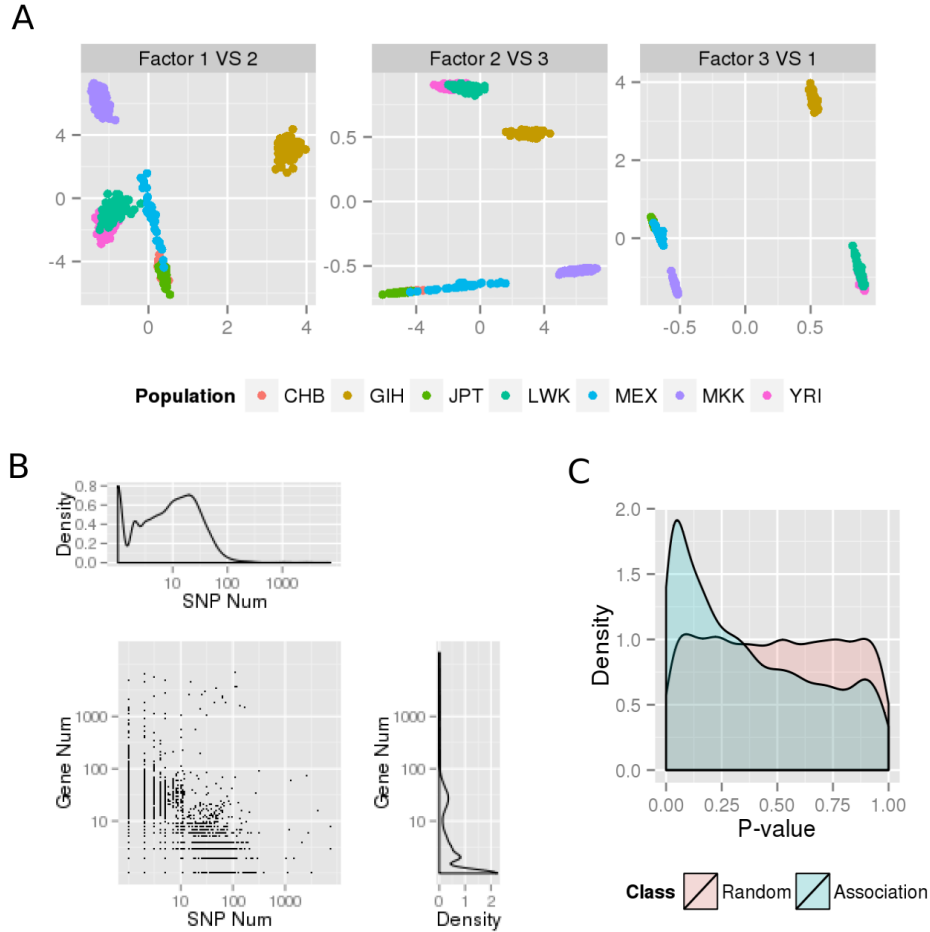


Figure 8: **Results of applying BGFA to HM3 data.** Panel A: The three dense factors specific to SNP data plotted against one another. The points represent individuals, and are colored according to population ancestry. The results are from one specific run with 1,093 factors listed in Table 6. Panel B: Plot of the number of SNPs and gene in sparse factors across 100 runs in log scale. Panel C: p -values for all SNP-gene pair appearing in the same sparse loadings are calculated using a univariate linear regression model with SNPs as predictors and gene expression levels as response (Association). For comparison, a non-included gene was randomly selected for each SNP-gene pair and p -values were calculated by treating the selected gene as the response (Random). These results are from one run with 1,093 factors.

methods did not recover results that well matched the sparsity levels of the simulated data. We then applied our model to data from two genomic studies. In the first application we applied BGFA to gene expression data with two observations. We found that BGFA recovered observation-specific covariance structure that captured co-varying genes that did not co-vary across observations. The sparse components recovered gene modules that were enriched for biologically meaningful functional annotations. These observation-specific sparse components were used to construct exposure-specific gene co-expression networks. In the second application, we used BGFA to identify eQTLs across three observations that included genotype data and gene expression levels. We found that the sparse loadings shared among genotype and gene expression observations were highly enriched for eQTL associations. Previous work has used two-step approaches to perform association mapping on low dimensional projections of high dimensional traits (Biswas et al., 2008; Gao et al., 2013); BGFA performs this association mapping in a single step, and the sparse solution allows the results to be interpretable, making clear which genes are affected by which SNPs. Furthermore, modeling high dimensional data (e.g., gene expression levels) jointly with relevant covariates (e.g., genotype data) enables ‘supervised’ dimension reduction: the covariate data guide the projection of the high dimensional data into a low dimensional space such that the mapping finds the latent space that is maximally shared with the covariates.

We anticipate our model will be used in a much wider context in other applications. Sample covariates such as age, sex, smoking status, or ethnicity may be included as an observation to identify a subset of genes that co-vary uniquely in females or smokers, for example. This model may be used to identify a set of topics in a scientific document corpus that maximally distinguish authors, journals, or institutions; another possible application is in the identification subsets of features about restaurants that are exclusive to their success or failure.

There are a number of directions left to explore more carefully in this model. First, we will consider the question of the identifiability of the recovered factor loadings with respect to the model specification and their sparsity, including developing estimates of significance of each of the recovered factors. Second, we will explore alternative methods for parameter estimation that both scale to much larger data sizes (e.g., for genome-wide association mapping of gene expression levels) and produce more robust results. We will also consider model averaging approaches that maintain interpretability but enable robust recovery of latent factors. Finally, we will consider model extensions that allow i) heterogeneous distributions of the residual error, which is currently Gaussian, and ii) vastly different numbers of features in each observation. While we saw in the results that BGFA produced meaningful results when the observations were heterogeneous (Bernoulli and Gaussian; different numbers of features), we believe that there are some model adaptations that will strengthen the application of BGFA to these types of study data.

Acknowledgments

The authors would like to thank David Dunson, and Sanvesh Srivastava for helpful discussions. BEE and CG were funded by NIH R00 HG006265 and NIH R01 MH101822. All

data are publicly available: the gene expression data were acquired through GEO GSE36868, and the genotype data were acquired through dbGaP, acquisition number phs000481, and generated from the Krauss Lab at the Children's Hospital Oakland Research Institute. This work was supported in part by U19 HL069757: Pharmacogenomics and Risk of Cardiovascular Disease. We acknowledge the PARC investigators and research team, supported by NHLBI, for collection of data from the Cholesterol and Pharmacogenetics clinical trial.

Appendix A. Markov chain Monte Carlo (MCMC) Algorithm for Posterior Inference

We first derive the MCMC algorithm with Gibbs sampling steps for the BGFA model. Write the joint distribution of the full BGFA model as

$$\begin{aligned} p(\mathbf{Y}, \mathbf{X}, \mathbf{\Lambda}, \mathbf{\Theta}, \mathbf{\Delta}, \mathbf{\Phi}, \mathbf{T}, \boldsymbol{\eta}, \boldsymbol{\gamma}, \mathbf{Z}, \boldsymbol{\Sigma}, \boldsymbol{\pi}) \\ = p(\mathbf{Y}|\mathbf{\Lambda}, \mathbf{X}, \boldsymbol{\Sigma})p(\mathbf{X}) \\ \times p(\mathbf{\Lambda}|\mathbf{\Theta})p(\mathbf{\Theta}|\mathbf{\Delta}, \mathbf{Z}, \mathbf{\Phi})p(\mathbf{\Delta}|\mathbf{\Phi})p(\mathbf{\Phi}|\mathbf{T})p(\mathbf{T}|\boldsymbol{\eta})p(\boldsymbol{\eta}|\boldsymbol{\gamma}) \\ \times p(\boldsymbol{\Sigma})p(\mathbf{Z}|\boldsymbol{\pi})p(\boldsymbol{\pi}), \end{aligned}$$

where $\mathbf{\Theta} = \{\theta_{jh}^{(w)}\}$, $\mathbf{\Delta} = \{\delta_{jh}^{(w)}\}$, $\mathbf{\Phi} = \{\phi_h^{(w)}\}$, $\mathbf{T} = \{\tau_h^{(w)}\}$, $\boldsymbol{\eta} = \{\eta^{(w)}\}$ and $\boldsymbol{\gamma} = \{\gamma^{(w)}\}$ are the collections of the global-factor-local \mathcal{TPB} prior parameters.

The full conditional distribution for latent factor \mathbf{x}_i is

$$\mathbf{x}_i|-\sim \mathcal{N}_k\left(\left(\mathbf{\Lambda}^T\boldsymbol{\Sigma}^{-1}\mathbf{\Lambda} + \mathbf{I}\right)^{-1}\mathbf{\Lambda}\boldsymbol{\Sigma}^{-1}\mathbf{y}_i, \left(\mathbf{\Lambda}^T\boldsymbol{\Sigma}^{-1}\mathbf{\Lambda} + \mathbf{I}\right)^{-1}\right),$$

for $i = 1, \dots, n$.

For $\mathbf{\Lambda}$, we derive the full conditional distributions of its p rows, $\boldsymbol{\lambda}_j$, for $j = 1 \dots p$.

$$\boldsymbol{\lambda}_j^T|-\sim \mathcal{N}_k\left(\left(\sigma_j^{-2}\mathbf{X}\mathbf{X}^T + \mathbf{D}_j^{-1}\right)^{-1}\sigma_j^{-2}\mathbf{X}\mathbf{y}_j^T, \left(\sigma_j^{-2}\mathbf{X}\mathbf{X}^T + \mathbf{D}_j^{-1}\right)^{-1}\right),$$

where

$$\mathbf{D}_j^{-1} = \text{diag}\left(\left(\theta_{j1}^{(w_j)}\right)^{I(z_1^{(w_j)}=1)}\left(\phi_1^{(w_j)}\right)^{I(z_1^{(w_j)}=0)}, \dots, \left(\theta_{jk}^{(w_j)}\right)^{I(z_k^{(w_j)}=1)}\left(\phi_k^{(w_j)}\right)^{I(z_k^{(w_j)}=0)}\right),$$

and w_j denotes the observation that the j^{th} row represents.

The full conditional distributions of $\theta_{jh}^{(w)}$, $\delta_{jh}^{(w)}$ and $\phi_h^{(w)}$ with $z_h^{(w)} = 1$ are

$$\begin{aligned} \theta_{jh}^{(w)}|-\sim \mathcal{GIG}(a - 1/2, 2\delta_{jh}^{(w)}, (\lambda_{jh}^{(w)})^2), \\ \delta_{jh}^{(w)}|-\sim \text{Ga}(a + b, \phi_h^{(w)} + \theta_{jh}^{(w)}), \\ \phi_h^{(w)}|-\sim \text{Ga}(p_w b + c, \sum_{j=1}^{p_w} \delta_{jh}^{(w)} + \tau_h^{(w)}), \end{aligned}$$

where \mathcal{GIG} is the generalized inverse Gaussian distribution.

The full conditional distribution of $\phi_h^{(w)}$ with $z_h^{(w)} = 0$ is

$$\phi_h^{(w)}|-\sim \mathcal{GIG}(c - p_w/2, 2\tau_h^{(w)}, \sum_{j=1}^{p_w} (\lambda_{jh}^{(w)})^2).$$

The full conditionals of the remaining parameters that we estimate are

$$\tau_h^{(w)}|-\sim \text{Ga}(c + d, \phi_h^{(w)} + \eta^{(w)}),$$

$$\begin{aligned}\eta^{(w)}|-\ &\sim Ga(kd + e, \gamma^{(w)} + \sum_{h=1}^k \tau_h^{(w)}), \\ \gamma^{(w)}|-\ &\sim Ga(e + f, \eta^{(w)} + \nu), \\ \pi^{(w)}|-\ &\sim Beta(1 + \sum_{h=1}^k z_h^{(w)}, 1 + k - \sum_{h=1}^k z_h^{(w)}).\end{aligned}$$

The full conditional distribution of $z_h^{(w)}$ is

$$\begin{aligned}\Pr(z_h^{(w)} = 1|-) &\propto \pi^{(w)} \prod_{j=1}^{p_w} \mathcal{N}(\lambda_{jh}^{(w)}; 0, \theta_{jh}^{(w)}) Ga(\theta_{jh}^{(w)}; a, \delta_{jh}^{(w)}) Ga(\delta_{jh}^{(w)}; b, \phi_h^{(w)}), \\ \Pr(z_h^{(w)} = 0|-) &\propto (1 - \pi^{(w)}) \prod_{j=1}^{p_w} \mathcal{N}(\lambda_{jh}^{(w)}; 0, \phi_h^{(w)}).\end{aligned}$$

We further integrate out $\delta_{jh}^{(w)}$ in $\Pr(z_h^{(w)} = 1| -)$:

$$\begin{aligned}\Pr(z_h^{(w)} = 1|-) &\propto \pi^{(w)} \prod_{j=1}^{p_w} \int \mathcal{N}(\lambda_{jh}^{(w)}; 0, \theta_{jh}^{(w)}) Ga(\theta_{jh}^{(w)}; a, \delta_{jh}^{(w)}) Ga(\delta_{jh}^{(w)}; b, \phi_h^{(w)}) d\delta_{jh}^{(w)} \\ &= \pi^{(w)} \prod_{j=1}^{p_w} \mathcal{N}(\lambda_{jh}^{(w)}; 0, \theta_{jh}^{(w)}) \frac{\Gamma(a+b)}{\Gamma(a)\Gamma(b)} \frac{(\theta_{jh}^{(w)})^{a-1} (\phi_h^{(w)})^b}{(\theta_{jh}^{(w)} + \phi_h^{(w)})^{a+b}}.\end{aligned}$$

The collapsed Gibbs sampler makes the sampling process more efficient (Liu, 1994). The full conditional of σ_j^{-2} for $j = 1, \dots, p$ is

$$\sigma_j^{-2}|-\ \sim Ga\left(n/2 + a_\sigma, 1/2(\mathbf{y}_j - \boldsymbol{\lambda}_j \mathbf{X})(\mathbf{y}_j - \boldsymbol{\lambda}_j \mathbf{X})^T + b_\sigma\right).$$

Appendix B. Variational Expectation Maximization (EM) Algorithm for MAP Parameter Estimates

Expectation Step: Given model parameters, the distribution of latent factor \mathbf{X} has shown in Appendix A. The expectation of the sufficient statistics of \mathbf{X} is derived as follows:

$$\begin{aligned}\langle \mathbf{x}_i \rangle &= (\boldsymbol{\Lambda}^T \boldsymbol{\Sigma}^{-1} \boldsymbol{\Lambda} + \mathbf{I})^{-1} \boldsymbol{\Lambda} \boldsymbol{\Sigma}^{-1} \mathbf{y}_i, \\ \langle \mathbf{x}_i \mathbf{x}_i^T \rangle &= \langle \mathbf{x}_i \rangle \langle \mathbf{x}_i \rangle^T + (\boldsymbol{\Lambda}^T \boldsymbol{\Sigma}^{-1} \boldsymbol{\Lambda} + \mathbf{I})^{-1}.\end{aligned}$$

The expectation of the indicator variable $\rho_h^{(w)} = \langle z_h^{(w)} \rangle$ is

$$\rho_h^{(w)} = \frac{\pi^{(w)} \prod_{j=1}^{p_w} \mathcal{N}(\lambda_{jh}^{(w)}; 0, \theta_{jh}^{(w)}) Ga(\theta_{jh}^{(w)}; a, \delta_{jh}^{(w)}) Ga(\delta_{jh}^{(w)}; b, \phi_h^{(w)})}{(1 - \pi^{(w)}) \prod_{j=1}^{p_w} \mathcal{N}(\lambda_{jh}^{(w)}; 0, \phi_h^{(w)}) + \pi^{(w)} \prod_{j=1}^{p_w} \mathcal{N}(\lambda_{jh}^{(w)}; 0, \theta_{jh}^{(w)}) Ga(\theta_{jh}^{(w)}; a, \delta_{jh}^{(w)}) Ga(\delta_{jh}^{(w)}; b, \phi_h^{(w)})}.$$

Maximization Step: The log posterior of $\boldsymbol{\Lambda}$ is written as

$$\log(p(\boldsymbol{\Lambda}| -)) \propto \text{tr}\left(\boldsymbol{\Sigma}^{-1} \boldsymbol{\Lambda} \mathbf{S}^{XY}\right) - \frac{1}{2} \text{tr}\left(\boldsymbol{\Lambda}^T \boldsymbol{\Sigma}^{-1} \boldsymbol{\Lambda} \mathbf{S}^{XX}\right) - \frac{1}{2} \sum_{h=1}^k \boldsymbol{\lambda}_h^T \mathbf{D}_h \boldsymbol{\lambda}_h,$$

where

$$\mathbf{D}_h = \text{diag}\left(\frac{\rho_h^{(1)}}{\theta_{1h}^{(1)}} + \frac{1 - \rho_h^{(1)}}{\phi_h^{(1)}}, \dots, \frac{\rho_h^{(m)}}{\theta_{p_m h}^{(m)}} + \frac{1 - \rho_h^{(m)}}{\phi_h^{(m)}}\right),$$

$$\mathbf{S}^{XY} = \sum_{i=1}^n \langle \mathbf{x}_{\cdot i} \rangle \mathbf{y}_{\cdot i}^T, \text{ and } \mathbf{S}^{XX} = \sum_{i=1}^n \langle \mathbf{x}_{\cdot i} \mathbf{x}_{\cdot i}^T \rangle.$$

We take the derivative with respect to the loading column $\boldsymbol{\lambda}_{\cdot h}$ to get the MAP estimate. For the first part in the right side of the proportion,

$$\begin{aligned} \frac{\partial \text{tr}(\boldsymbol{\Sigma}^{-1} \boldsymbol{\Lambda} \mathbf{S}^{XY})}{\partial \boldsymbol{\lambda}_{\cdot h}} &= (\mathbf{1}_k^h \otimes \mathbf{I}_p) \times \text{vec}[\boldsymbol{\Sigma}^{-1} \mathbf{S}^{YX}] = \text{vec}\left(\boldsymbol{\Sigma}^{-1} \mathbf{S}^{YX} \mathbf{1}_k^h\right) \\ &= \boldsymbol{\Sigma}^{-1} \mathbf{S}^{YX} \mathbf{1}_k^h, \end{aligned}$$

where vec is vectorization operation of a matrix, $\mathbf{1}_k^h \in \mathbb{R}^{k \times 1}$ is a zero vector except h^{th} row being 1, and $\mathbf{S}^{YX} = (\mathbf{S}^{XY})^T$. For the second part,

$$\begin{aligned} \frac{\partial \text{tr}(\boldsymbol{\Lambda}^T \boldsymbol{\Sigma}^{-1} \boldsymbol{\Lambda} \mathbf{S}^{XX})}{\partial \boldsymbol{\lambda}_{\cdot h}} &= 2(\mathbf{1}_k^h \otimes \mathbf{I}_p) \times \text{vec}[\boldsymbol{\Sigma}^{-1} \boldsymbol{\Lambda} \mathbf{S}^{XX}] = 2 \text{vec}\left(\boldsymbol{\Sigma}^{-1} \boldsymbol{\Lambda} \mathbf{S}^{XX} \mathbf{1}_k^h\right) \\ &= 2 \boldsymbol{\Sigma}^{-1} \boldsymbol{\Lambda} \mathbf{S}^{XX} \mathbf{1}_k^h. \end{aligned}$$

For the third part, the derivative is $\mathbf{D}_h \boldsymbol{\lambda}_{\cdot h}$. The MAP of $\boldsymbol{\lambda}_{\cdot h}$ is obtained by setting the derivative to zero:

$$\hat{\boldsymbol{\lambda}}_{\cdot h} = [\mathbf{S}_{hh}^{XX} \mathbf{I}_p + \boldsymbol{\Sigma} \mathbf{D}_h]^{-1} \left(\mathbf{S}_{\cdot h}^{YX} - \sum_{h' \neq h} \boldsymbol{\lambda}_{\cdot h'} \mathbf{S}_{h'h}^{XX} \right),$$

where \mathbf{S}_{ij}^{XX} is the $(i, j)^{\text{th}}$ element of \mathbf{S}^{XX} , and $\mathbf{S}_{\cdot h}^{YX}$ is the h^{th} column of \mathbf{S}^{YX} . The matrix to be inverted is a diagonal matrix, so $\hat{\boldsymbol{\lambda}}_{\cdot h}$ is calculated efficiently. The MAP estimates of the other model parameters are obtained straightforwardly from their full conditional distributions with variables replaced by their expectations. We list the parameter updates for those variables here:

$$\begin{aligned} \hat{\theta}_{jh}^{(w)} &= \frac{2a - 3 + \sqrt{(2a - 3)^2 + 8(\lambda_{jh}^{(w)})^2 \delta_{jh}^{(w)}}}{4\delta_{jh}^{(w)}}, \\ \hat{\delta}_{jh}^{(w)} &= \frac{a + b}{\theta_{jh}^{(w)} + \phi_h^{(w)}}, \\ \hat{\phi}_h^{(w)} &= \frac{p' - 1 + \sqrt{(p' - 1)^2 + a'b'}}{a'}, \text{ with} \\ p' &= \rho_h^{(w)} p_w b - (1 - \rho_h^{(w)}) p_w / 2 + c, \\ a' &= 2(\rho_h^{(w)} \sum_{j=1}^{p_w} \delta_{jh}^{(w)} + \tau_h^{(w)}), b' = (1 - \rho_h^{(w)}) \sum_{j=1}^{p_w} (\lambda_{jh}^{(w)})^2 \end{aligned}$$

$$\begin{aligned}\hat{\tau}_h^{(w)} &= \frac{c + d}{\phi_h^{(w)} + \eta^{(w)}}, \\ \hat{\eta}^{(w)} &= \frac{dk + e}{\gamma^{(w)} + \sum_{h=1}^k \tau_h^{(w)}}, \\ \hat{\gamma}^{(w)} &= \frac{e + f}{\eta^{(w)} + \nu}, \\ \hat{\pi}^{(w)} &= \frac{\sum_{h=1}^k \rho_h^{(w)}}{k}, \\ \hat{\sigma}_j^{-2} &= \frac{n/2 + a_\sigma - 1}{1/2(\mathbf{y}_j - \boldsymbol{\lambda}_j \langle \mathbf{X} \rangle)(\mathbf{y}_j - \boldsymbol{\lambda}_j \langle \mathbf{X} \rangle)^T + b_\sigma}.\end{aligned}$$

References

- Christophe Andrieu, Nando De Freitas, Arnaud Doucet, and Michael I. Jordan. An introduction to MCMC for machine learning. *Machine learning*, 50(1-2):5–43, 2003.
- Cdric Archambeau and Francis Bach. Sparse probabilistic projections. In *NIPS*, pages 73–80, 2008.
- Artin Armagan, David Dunson, and Jaeyong Lee. Generalized double pareto shrinkage. *arXiv preprint arXiv:1104.0861*, 2011a.
- Artin Armagan, David B. Dunson, and Merlise Clyde. Generalized beta mixtures of gaussians. *arXiv preprint arXiv:1107.4976*, 2011b.
- Francis R. Bach and Michael I. Jordan. A probabilistic interpretation of canonical correlation analysis. *Technical Report 688, Department of Statistics, University of California, Berkeley*, 2005.
- A. Bhattacharya and D. B. Dunson. Sparse bayesian infinite factor models. *Biometrika*, 98(2):291–306, 2011.
- Anirban Bhattacharya, Debdeep Pati, Natesh S. Pillai, and David B. Dunson. Bayesian shrinkage. *arXiv preprint arXiv:1212.6088*, 2012.
- Shameek Biswas, John D. Storey, and Joshua M. Akey. Mapping gene expression quantitative trait loci by singular value decomposition and independent component analysis. *BMC Bioinformatics*, 9(1):244, 2008.
- Christopher D. Brown, Lara M. Mangravite, and Barbara E. Engelhardt. Integrative modeling of eQTLs and cis-regulatory elements suggests mechanisms underlying cell type specificity of eQTLs. *PLoS Genetics*, 9(8):e1003649, 2013.
- M. W. Browne. The maximum-likelihood solution in inter-battery factor analysis. *British Journal of Mathematical and Statistical Psychology*, 32(1):75–86, 1979.

- Carlos M. Carvalho, Jeffrey Chang, Joseph E. Lucas, Joseph R. Nevins, Quanli Wang, and Mike West. High-dimensional sparse factor modeling: applications in gene expression genomics. *Journal of the American Statistical Association*, 103(484), 2008.
- Carlos M. Carvalho, Nicholas G. Polson, and James G. Scott. Handling sparsity via the horseshoe. In *International Conference on Artificial Intelligence and Statistics*, pages 73–80, 2009.
- Carlos M. Carvalho, Nicholas G. Polson, and James G. Scott. The horseshoe estimator for sparse signals. *Biometrika*, 97(2):465–480, 2010.
- Pierre Comon. Independent component analysis, a new concept? *Signal processing*, 36(3): 287–314, 1994.
- John P Cunningham and Zoubin Ghahramani. Unifying linear dimensionality reduction. *arXiv preprint arXiv:1406.0873*, 2014.
- Arthur P. Dempster, Nan M. Laird, and Donald B. Rubin. Maximum likelihood from incomplete data via the EM algorithm. *Journal of the Royal Statistical Society. Series B (Methodological)*, pages 1–38, 1977.
- David Edwards. *Introduction to Graphical Modelling*. Springer, New York, 2nd edition edition, June 2000. ISBN 9780387950549.
- Barbara E. Engelhardt and Ryan P. Adams. Bayesian structured sparsity from gaussian fields. *arXiv preprint arXiv:1407.2235*, 2014.
- Barbara E. Engelhardt and Matthew Stephens. Analysis of population structure: A unifying framework and novel methods based on sparse factor analysis. *PLoS Genetics*, 6(9): e1001117, 2010.
- Chuan Gao, Christopher D. Brown, and Barbara E. Engelhardt. A latent factor model with a mixture of sparse and dense factors to model gene expression data with confounding effects. *arXiv:1310.4792 [q-bio, stat]*, October 2013.
- Chuan Gao, Shiwen Zhao, Ian C McDowell, Christopher D. Brown, and Barbara E. Engelhardt. Differential gene co-expression networks via bayesian biclustering models. *arXiv:1411.1997*, November 2014.
- Zoubin Ghahramani, Thomas L. Griffiths, and Peter Sollich. Bayesian nonparametric latent feature models. In *Bayesian Statistics*, pages 201–225. Oxford University Press, 2007.
- Ignacio Gonzalez, Sbastien Djean, Pascal GP Martin, and Alain Baccini. CCA: an r package to extend canonical correlation analysis. *Journal of Statistical Software*, 23(12):1–14, 2008.
- Chris Hans. Bayesian lasso regression. *Biometrika*, 96(4):835–845, 2009.
- Arthur E. Hoerl and Robert W. Kennard. Ridge regression: Biased estimation for nonorthogonal problems. *Technometrics*, 12(1):55–67, 1970.

- Harold Hotelling. Analysis of a complex of statistical variables into principal components. *Journal of educational psychology*, 24(6):417, 1933.
- Harold Hotelling. Relations between two sets of variates. *Biometrika*, pages 321–377, 1936.
- Da Wei Huang, Brad T. Sherman, and Richard A. Lempicki. Systematic and integrative analysis of large gene lists using DAVID bioinformatics resources. *Nature Protocols*, 4(1): 44–57, 2009.
- Junzhou Huang, Tong Zhang, and Dimitris Metaxas. Learning with structured sparsity. *The Journal of Machine Learning Research*, 12:3371–3412, 2011.
- Rodolphe Jenatton, Guillaume Obozinski, and Francis Bach. Structured sparse principal component analysis. *arXiv preprint arXiv:0909.1440*, 2009.
- Rodolphe Jenatton, Jean-Yves Audibert, and Francis Bach. Structured variable selection with sparsity-inducing norms. *The Journal of Machine Learning Research*, 12:2777–2824, 2011.
- Yangqing Jia, Mathieu Salzmann, and Trevor Darrell. Factorized latent spaces with structured sparsity. In *Advances in Neural Information Processing Systems*, pages 982–990, 2010.
- Arto Klami and Samuel Kaski. Probabilistic approach to detecting dependencies between data sets. *Neurocomputing*, 72(1):39–46, 2008.
- Arto Klami, Seppo Virtanen, and Samuel Kaski. Bayesian canonical correlation analysis. *Journal of Machine Learning Research*, 14:965–1003, 2013.
- David Knowles and Zoubin Ghahramani. Nonparametric bayesian sparse factor models with application to gene expression modeling. *The Annals of Applied Statistics*, 5(2B): 1534–1552, 2011.
- Daphne Koller and Nir Friedman. *Probabilistic Graphical Models: Principles and Techniques*. The MIT Press, 1 edition, July 2009.
- Matthieu Kowalski. Sparse regression using mixed norms. *Applied and Computational Harmonic Analysis*, 27(3):303–324, 2009.
- Matthieu Kowalski and Bruno Torrsani. Structured sparsity: from mixed norms to structured shrinkage. In *SPARS’09-Signal Processing with Adaptive Sparse Structured Representations*, 2009.
- Minjung Kyung, Jeff Gill, Malay Ghosh, and George Casella. Penalized regression, standard errors, and bayesian lassos. *Bayesian Analysis*, 5(2):369–411, 2010.
- Sang Hong Lee, Jian Yang, Michael E. Goddard, Peter M. Visscher, and Naomi R. Wray. Estimation of pleiotropy between complex diseases using single-nucleotide polymorphism-derived genomic relationships and restricted maximum likelihood. *Bioinformatics*, 28(19): 2540–2542, 2012.

- Jeffrey T. Leek, Robert B. Scharpf, Hector Corrada Bravo, David Simcha, Benjamin Langmead, W. Evan Johnson, Donald Geman, Keith Baggerly, and Rafael A. Irizarry. Tackling the widespread and critical impact of batch effects in high-throughput data. *Nature Reviews Genetics*, 11(10):733–739, October 2010. ISSN 1471-0056. doi: 10.1038/nrg2825.
- Jun S. Liu. The collapsed gibbs sampler in bayesian computations with applications to a gene regulation problem. *Journal of the American Statistical Association*, 89(427): 958–966, 1994.
- Joseph E. Lucas, Hsiu-Ni Kung, and Jen-Tsan A. Chi. Latent factor analysis to discover pathway-associated putative segmental aneuploidies in human cancers. *PLoS Computational Biology*, 6(9):e1000920, 2010.
- Lara M Mangravite, Barbara E Engelhardt, Marisa W Medina, Joshua D Smith, Christopher D Brown, Daniel I Chasman, Brigham H Mecham, Bryan Howie, Heejung Shim, Devesh Naidoo, et al. A statin-dependent qtl for *GATM* expression is associated with statin-induced myopathy. *Nature*, 2013.
- Toby J. Mitchell and John J. Beauchamp. Bayesian variable selection in linear regression. *Journal of the American Statistical Association*, 83(404):1023–1032, 1988.
- Radford M. Neal. *Bayesian learning for neural networks*. PhD thesis, University of Toronto, 1995.
- John Novembre and Matthew Stephens. Interpreting principal component analyses of spatial population genetic variation. *Nature Genetics*, 40(5):646–649, 2008.
- Anthony O’Hagan. On outlier rejection phenomena in bayes inference. *Journal of the Royal Statistical Society. Series B (Methodological)*, pages 358–367, 1979.
- Trevor Park and George Casella. The bayesian lasso. *Journal of the American Statistical Association*, 103(482):681–686, 2008.
- Nicholas G. Polson and James G. Scott. Shrink globally, act locally: sparse bayesian regularization and prediction. *Bayesian Statistics*, 9:501–538, 2010.
- Iosifina Pournara and Lorenz Wernisch. Factor analysis for gene regulatory networks and transcription factor activity profiles. *BMC Bioinformatics*, 8:61, 2007.
- Alkes L. Price, Nick J. Patterson, Robert M. Plenge, Michael E. Weinblatt, Nancy A. Shadick, and David Reich. Principal components analysis corrects for stratification in genome-wide association studies. *Nature Genetics*, 38(8):904–909, 2006.
- Iulian Pruteanu-Malinici, Daniel L. Mace, and Uwe Ohler. Automatic annotation of spatial expression patterns via sparse bayesian factor models. *PLoS Computational Biology*, 7(7):e1002098, 2011.
- J.K. Romberg, Hyeokho Choi, and R.G. Baraniuk. Bayesian tree-structured image modeling using wavelet-domain hidden markov models. *IEEE Transactions on Image Processing*, 10(7):1056–1068, 2001.

- Sam Roweis. EM algorithms for PCA and SPCA. *Advances in neural information processing systems*, pages 626–632, 1998.
- Konstantin Salomatin, Yiming Yang, and Abhimanyu Lad. Multi-field correlated topic modeling. In *SDM*, pages 628–637, 2009.
- Mathieu Salzmann, Carl H. Ek, Raquel Urtasun, and Trevor Darrell. Factorized orthogonal latent spaces. In *International Conference on Artificial Intelligence and Statistics*, pages 701–708, 2010.
- Juliane Schfer and Korbinian Strimmer. An empirical bayes approach to inferring large-scale gene association networks. *Bioinformatics*, 21(6):754–764, 2005.
- Matthew Stephens. Dealing with label switching in mixture models. *Journal of the Royal Statistical Society: Series B (Statistical Methodology)*, 62(4):795–809, 2000.
- Matthew Stephens. A unified framework for association analysis with multiple related phenotypes. *PLoS ONE*, 8(7):e65245, 2013.
- Matthew Stephens and David J. Balding. Bayesian statistical methods for genetic association studies. *Nature Reviews Genetics*, 10(10):681–690, 2009.
- Barbara E. Stranger, Stephen B. Montgomery, Antigone S. Dimas, Leopold Parts, Oliver Stegle, Catherine E. Ingle, Magda Sekowska, George Davey Smith, David Evans, Maria Gutierrez-Arcelus, Alkes Price, Towfique Raj, James Nisbett, Alexandra C. Nica, Claude Beazley, Richard Durbin, Panos Deloukas, and Emmanouil T. Dermitzakis. Patterns of cis regulatory variation in diverse human populations. *PLoS Genetics*, 8(4):e1002639, 2012.
- Robert Tibshirani. Regression shrinkage and selection via the lasso. *Journal of the Royal Statistical Society. Series B (Methodological)*, pages 267–288, 1996.
- Michael E. Tipping. Sparse bayesian learning and the relevance vector machine. *The Journal of Machine Learning Research*, 1:211–244, 2001.
- Michael E. Tipping and Christopher M. Bishop. Mixtures of probabilistic principal component analyzers. *Neural computation*, 11(2):443–482, 1999a.
- Michael E. Tipping and Christopher M. Bishop. Probabilistic principal component analysis. *Journal of the Royal Statistical Society: Series B (Statistical Methodology)*, 61(3):611–622, 1999b.
- Seppo Virtanen, Arto Klami, Suleiman A. Khan, and Samuel Kaski. Bayesian group factor analysis. *arXiv preprint arXiv:1110.3204*, 2011.
- Zaiwen Wen and Wotao Yin. A feasible method for optimization with orthogonality constraints. *Mathematical Programming*, 142(1-2):397–434, 2013.
- Mike West. On scale mixtures of normal distributions. *Biometrika*, 74(3):646–648, 1987.

- Mike West. Bayesian factor regression models in the large p, small n paradigm. *Bayesian statistics*, 7(2003):723–732, 2003.
- Daniela Witten, Rob Tibshirani, Sam Gross, and Balasubramanian Narasimhan. *PMA: Penalized Multivariate Analysis*, 2013. URL <http://CRAN.R-project.org/package=PMA>. R package version 1.0.9.
- Daniela M. Witten and Robert J. Tibshirani. Extensions of sparse canonical correlation analysis with applications to genomic data. *Statistical applications in genetics and molecular biology*, 8(1):1–27, 2009.
- Daniela M. Witten, Robert Tibshirani, and Trevor Hastie. A penalized matrix decomposition, with applications to sparse principal components and canonical correlation analysis. *Biostatistics*, 10(3):515–534, 2009.
- Ming Yuan and Yi Lin. Model selection and estimation in regression with grouped variables. *Journal of the Royal Statistical Society: Series B (Statistical Methodology)*, 68(1):49–67, 2006.
- W. Zhang, J. Zhu, E.E. Schadt, and J.S. Liu. A bayesian partition method for detecting pleiotropic and epistatic eQTL modules. *PLoS Computational Biology*, 6(1):e1000642, 2010.
- Peng Zhao, Guilherme Rocha, and Bin Yu. The composite absolute penalties family for grouped and hierarchical variable selection. *The Annals of Statistics*, 37(6A):3468–3497, 2009.
- Hui Zou and Trevor Hastie. Regularization and variable selection via the elastic net. *Journal of the Royal Statistical Society. Series B (Statistical Methodology)*, 67(2):301–320, 2005.
- Hui Zou, Trevor Hastie, and Robert Tibshirani. Sparse principal component analysis. *Journal of computational and graphical statistics*, 15(2):265–286, 2006.